RADIATION FIELDS OF A COMPLEX SOURCE IN 2-D CIRCULAR RADOME WITH METAL GRATINGS

A THESIS

SUBMITTED TO THE DEPARTMENT OF ELECTRICAL AND

ELECTRONICS ENGINEERING

AND THE INSTITUTE OF ENGINEERING AND SCIENCES

OF BILKENT UNIVERSITY

IN PARTIAL FULFILLMENT OF THE REQUIREMENTS

FOR THE DEGREE OF

MASTER OF SCIENCE

By
Slim Ouardani
August 1997

RADIATION FIELDS OF A COMPLEX SOURCE IN 2-D CIRCULAR RADOME WITH METAL GRATINGS

A THESIS

SUBMITTED TO THE DEPARTMENT OF ELECTRICAL AND

ELECTRONICS ENGINEERING

AND THE INSTITUTE OF ENGINEERING AND SCIENCES

OF BILKENT UNIVERSITY

IN PARTIAL FULFILLMENT OF THE REQUIREMENTS

FOR THE DEGREE OF
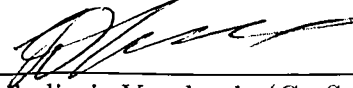
MASTER OF SCIENCE

By

Slim Ouardani

August 1997

I certify that I have read this thesis and that in my opinion it is fully adequate, in scope and in quality, as a thesis for the degree of Master of Science.
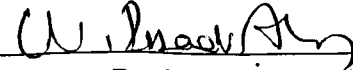
Prof. Dr. Ayhan Altıntaş(Supervisor)

I certify that I have read this thesis and that in my opinion it is fully adequate, in scope and in quality, as a thesis for the degree of Master of Science.
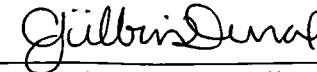
Dr. Vladimir Yurchenko(Co-Supervisor)

I certify that I have read this thesis and that in my opinion it is fully adequate, in scope and in quality, as a thesis for the degree of Master of Science.

Assoc. Prof. Dr. İrşadi Aksun

I certify that I have read this thesis and that in my opinion it is fully adequate, in scope and in quality, as a thesis for the degree of Master of Science.
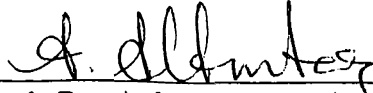
Assoc. Prof. Dr. Gülbin Dural

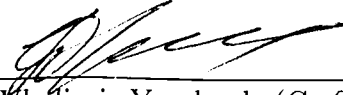Approved for the Institute of Engineering and Sciences:

Prof. Dr. Mehmet Baray
Director of Institute of Engineering and Sciences

I certify that I have read this thesis and that in my opinion it is fully adequate, in scope and in quality, as a thesis for the degree of Master of Science.
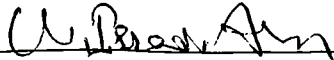
_____
Prof. Dr. Ayhan Altıntaş(Supervisor)

I certify that I have read this thesis and that in my opinion it is fully adequate, in scope and in quality, as a thesis for the degree of Master of Science.
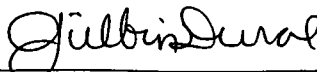
_____
Dr. Vladimir Yurchenko(Co-Supervisor)

I certify that I have read this thesis and that in my opinion it is fully adequate, in scope and in quality, as a thesis for the degree of Master of Science.

_____
Assoc. Prof. Dr. İrşadi Aksun

I certify that I have read this thesis and that in my opinion it is fully adequate, in scope and in quality, as a thesis for the degree of Master of Science.

_____
Assoc. Prof. Dr. Gülbin Dural

Approved for the Institute of Engineering and Sciences:

_____
Prof. Dr. Mehmet Baray
Director of Institute of Engineering and Sciences

ABSTRACT

RADIATION FIELDS OF A COMPLEX SOURCE IN 2-D CIRCULAR RADOME WITH METAL GRATINGS

Slim Ouardani

M.S. in Electrical and Electronics Engineering

Supervisors:
Prof. Dr. Ayhan Altıntaş
Dr. Vladimir Yurchenko

August 1997

In this thesis, the transmission effect of a two-dimensional circular radome with periodic metal gratings is analyzed. We started with the study of gratings consisting of periodic arrays of thin lossy strips surrounded by vacuum. Then we investigated the behavior of such gratings if a dielectric layer is inserted between them. Complex line sources are considered to simulate directed beam fields used in practice. The fields on the interior and exterior sides of the radome are represented by modal cylindrical waves. Taking advantage of theoretical considerations recently published, we propose an approximate method and stress the numerical aspect. Data is obtained for the far field solutions and the directivity, and their dependences on different radome parameters. It appears that directivity variations with beam orientation are decreased considerably by a proper insertion of the dielectric layer.

Keywords : Dielectric radome, metal gratings, directivity.

ÖZET

İKİ BOYUTLU METAL IZGARALI DAİRESEL RADOM İÇİNDEKİ BİR KARMAŞIK KAYNAĞIN IŞINIMI

Slim Ouardani
Elektrik ve Elektronik Mühendisliği Bölümü Yüksek Lisans

Tez Yöneticileri:
Prof. Dr. Ayhan Altıntaş
Dr. Vladimir Yurchenko

Ağustos 1997

Bu tezde, iki boyutlu, periodik metal ızgaralı dairesel radomların alan geçirgenliği incelenmiştir. Öncelikle, ızgaraların periodik ve kayıplı olduğu ve çevrelerinde ayrıca yalıtkan olmadığı durum incelenmiş, daha sonra bu ızgaralın arasına yalıtkan tabaka konulması durumu çözülmüştür. Pratikte kullanılan yönlü hüzme kaynağının benzetimi için karmaşık noktaya yerleştirilmiş kaynak modeli kullanılmıştır. Çözüm için metal ızgara ve yalıtkan tabakadan oluşan radom geometrisinin içinde ve dışındaki alanlar silindirik dalgalar şeklinde yazılmıştır. Daha sonra literatürdeki son katkılardan esinlenilerek yaklaşık ama nümerik olarak verimli bir yöntem uygulanmıştır. Işınım alanının değişik radom parametleri ile değişimi hususunda veriler elde edilmiştir. Bu verilere göre hüzme kazancının, hüzmenin yönüe göre değişmesi, metal ızgara arasına konulan yalıtkan levha ile kontrol edilebilmektedir.

Anahtar Kelimeler : Yalıtkan radom, metal ızgaralar, ışımın kazancı

ACKNOWLEDGEMENT

To my family.

Contents

List of Figures

Chapter 1

INTRODUCTION

The transmission and reflection of the wave propagating through single and multiple dielectric layer systems is always an interesting subject of study which finds many applications. These systems have been studied since the early development of the wave propagation, especially the electromagnetic waves. The layers can be planar, cylindrical or spherical, of non uniform thickness, open or closed in the form of shells.

Open layers may affect the propagation process by transmission through or guiding within them; closed layers may exhibit, in addition, phenomena attributable to resonance, either inside the layers themselves or in the cavity enclosed by the layers. One of the most important applications of the multiple dielectric layer systems is the Fabry-Parot interferometer which has been used in the optical spectrum analyzer for a long time. When the dielectric layers are stacked in a periodic manner, a special class of layered media which exhibits many interesting phenomena has been found to be very useful. The examples are the Bragg reflector and various filters, such as frequency selective filters, which are capable of modifying the transmission within a certain range of frequency.

Theory of planarly layered media is a classical example which is found in textbooks, however that of cylindrically and spherically layered media was done

not long ago[1]. The concentration was on the scattering of point sources by curved layers with special interest in the cylindrical and spherical structures.

The effect of a cylindrical dielectric layer on the penetration of electromagnetic waves has been extensively analyzed for the last few years, due to its potential applications such as in the study of the performance of a radar antenna enclosed by a radome. A radome is a dielectric shell which is used to protect the radar from rain, wind, sun, etc. In the presence of the radome, the radiation pattern of the radar antenna is distorted and a shift in the beam pointing angle of the radar appears [2].In practice, a precise analysis of radome performance is difficult, and nearly impossible, because the general shape of the radome layer does not fit into the frame suitable for exact analysis. One must therefore resort to some approximation methods. The basic principle of approximation is to find a canonical configuration to approximate the surface of the dielectric layer. In [2] a method of modal cylindrical wave spectrum, which is an extension of the plane wave spectrum surface integration technique [3], is applied to the analysis of a two-dimensional elliptic radome. In [4] analysis of two-dimensional circular dielectric layer was performed to account for the curvature effect which was ignored in the previous studies, and correct slab transmission coefficient that improve local plane slab hypothesis was found. Propagation of Gaussian beam through dielectric plane layer [5] and circular cylindrical layer [6] was analyzed. Narrow beam has been employed as basis elements in the synthesis procedure, and each beam element has been propagated through the layer to the observer by non uniform complex ray asymptotics. In [7] equivalence partial angular harmonic and ray-type Green's functions were investigated focusing on the relation between periodic and non periodic Green's functions for a closed $(0 < \theta < 2\pi)$ and open $(-\infty < \theta < \infty)$ shell, respectively. Far field solutions for real and complex line sources enclosed by a two-dimensional circular radome are obtained in [8]. Cylindrical functions are used to represent the incident field and the scattered fields in the inner, middle, and outer regions. Boundary conditions are applied to the fields and analytical solutions to the problem is obtained.

Several types of boundary conditions have been developed for layered sheets to calculate the fields scattered or radiated by systems of thin layers. If the layers are modeled as infinitesimally thin structures described in terms of a set

of boundary conditions, the computational problem becomes much less intense. Generalized impedance boundary conditions are derived for planar, magnetic dielectric slab grounded by a perfect electric conducting plane and for a magnetic dielectric coated perfect electric conducting cylinder [9]. Generalized resistive boundary conditions are also obtained for a planar, transparent dielectric slab. Other types of boundary conditions and the corresponding integral equations apply to penetrable sheets, and they are described as transmission boundary conditions. Curvature corrected boundary conditions for combined resistive and conductive sheets are described in [10]. In [11], attention was focused in the case of a layered sheet with different reflection properties characterizing its two faces. The boundary conditions involve only the tangential components of the fields and a set of the corresponding surface integral equations is provided for impenetrable and penetrable sheets. These boundary conditions can also reduce to the special case of sheets with identical reflection coefficients from both sides.

So far, a brief review of the problem of electromagnetic wave penetration through dielectric layer is given. In recent years the diffraction analysis of electromagnetic waves by dielectric gratings have been intensively investigated as well. Nowadays such structures are gaining widespread use as in frequency selective filters, radomes and polarizers. In [12] the problem of scattering from a resistive grating is formulated in the spectral domain, where the convolution form of the integral equation for the scattered field reduces to a product form which can be solved by moment method techniques. Resistive boundary conditions are used with a constant surface resistance defined for the strips that are thin compared to the attenuation length. The transmission and reflection coefficients of the array of strips are determined from the scattered fields. Later this approach was extended to multi-layered resistive strip gratings [13], and in [14] the study of gratings consisting of a periodic array of thin lossy strips with arbitrary cross section is provided.

In this study, the effect of a two-dimensional circular radome with metal gratings, on the propagation of electromagnetic fields radiated by a complex line source is investigated. The fields on the concave and convex sides of the radome are represented by modal cylindrical waves. Boundary conditions provided in

[11] are used to derive the analytic solution of the problem. At first, the transmission effect of circular gratings consisting of periodic arrays of lossy strips is considered. Two cases are described,high conductive (non-perfect metal) and high resistive (poor dielectric) thin strips. Finally the original problem is analyzed. Although we employed approximate boundary conditions to establish the field on the exterior side of the radome due to the source located on the interior side, the numerical data obtained justify strongly the validity of the method. Another important thing is that the method is effective for any number (≥ 1) of the strips with any angular width from 0 to 2π. This enables us to simulate different structures already studied in literature such as reflector antennas [15] and 2-D circular dielectric radome [8], and compare with the techniques used to solve for these geometries. The size of the matrix is determined by the radius of curvature and fairly large structures can be treated with guaranteed accuracy. Numerical results for the far fields and directivity of various structures are obtained. Thickness variations are also included to give a better understanding of the models. Comparisons are given to study the validity of the method.

The outline of this thesis is as follows: In chapter 2 we introduce the basic concept of the method and the formulation of the problem. Numerical results are presented in chapter 3. Main conclusions follow in chapter 4.

Throughout the analysis, a sinusoidally-varying time dependence $e^{-i\omega t}$ is assumed and suppressed.

Chapter 2

ANALYSIS OF TRANSMISSION THROUGH A RADOME WITH METAL GRATINGS

In this analysis, complex line source is considered to simulate directed beam fields. The primary wave fields are represented as expansion series of cylindrical waves, and then the effect of transmission through the radome is analyzed to evaluate the radiation fields. Formulation of the problem is carried out for thin periodic metal gratings and then extended to the case of periodic metal-dielectric radome.

2.1 Radiation Through a Circular Radome of a Thin Periodic Metal Grating

In Figure 2.1 a line source is placed at the complex position $\vec{r}_s$ which is given by

$$\vec{r}_s = \vec{r}_0 + i\vec{b} = r_0\hat{x} + ib(cos\beta\hat{x} + sin\beta\hat{y}) \tag{2.1}$$

where the parameter b is a measure of the source directivity, and the angle β represents the direction of the beam.
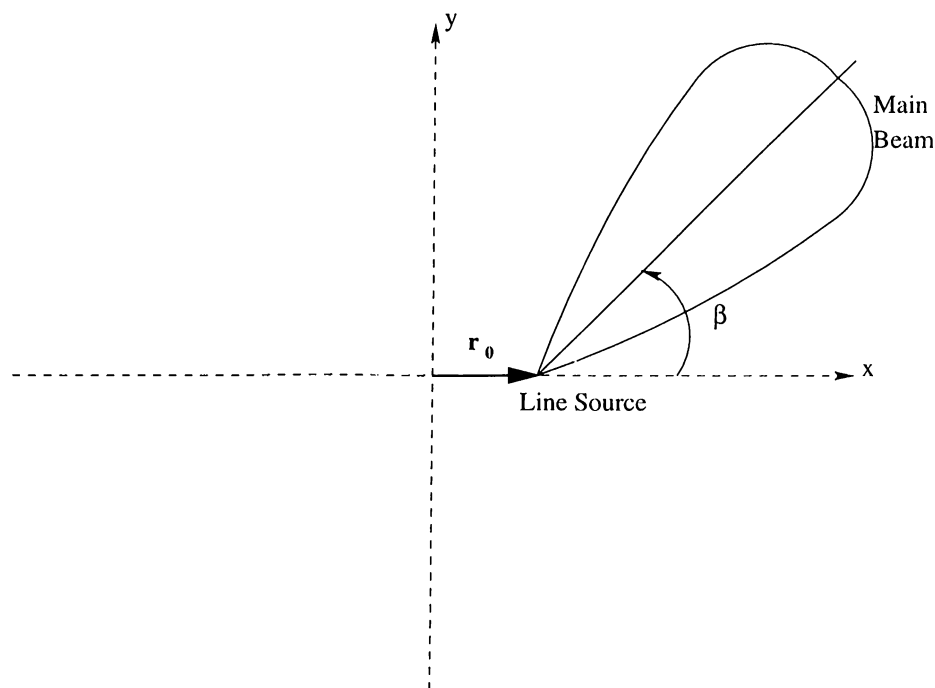
Figure 2.1: Geometry of the complex line source

Depending on the polarization, we denote by $U(\vec{r})$ the E_z or H_z of the fields. The incident field due to the line source of amplitude C at the complex position $\vec{r}_s$ is given by:

$$U^{inc}(\vec{r}) = CH_0^{(1)}(k_0 \mid \vec{r} - \vec{r}_s \mid) \tag{2.2}$$

where k_0 is the free space wave number and $H_0^1(Kr)$ is the Hankel function of the first kind. By the addition theorem for the Hankel function, we can write (2.2)

as

$$U^{inc}(r, \phi) = C \sum_n J_n(k_0 r_s) H_n^{(1)}(k_0 r) e^{in(\phi - \theta_s)}, r > |r_s| \tag{2.3}$$

where

$$r_s = \sqrt{r_0^2 - b^2 + 2ibr_0 cos\beta} \tag{2.4}$$

$$\theta_s = cos^{-1}(\frac{r_0 + ibcos\beta}{r_s}) \tag{2.5}$$
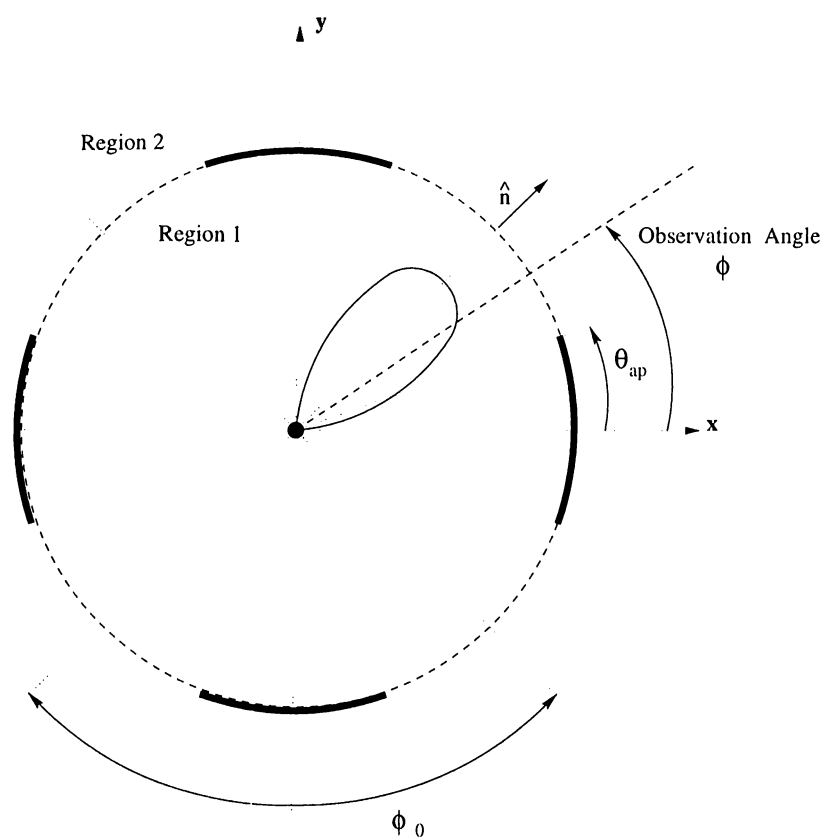
Figure 2.2: Geometry of circular periodic metal gratings

Figure 2.2 shows a grating consisting of an array of circular thin metal strips surrounded by vacuum. The perfectly conducting strips have zero thickness and angular width $2\theta_{ap}$. The array is periodic with period ϕ_0. To solve the problem of a complex line source radiating through periodic metal grating, the scattered field should satisfy the Helmholtz equation, the Neumann or Dirichlet type boundary

condition on the strips, the continuity condition at the slots and the radiation condition at infinity. The scattered field can be expressed in integral form by imposing the boundary condition as follows

$$- U^{inc}(\vec{r}, \vec{r'}) = \int_M J_E(\vec{r'}) G_0(\vec{r}, \vec{r'}) d\vec{r'}, \vec{r} \in M \tag{2.6}$$

in E-polarization

$$- \frac{\partial U^{inc}(\vec{r})}{\partial n} = \frac{\partial}{\partial n} \int_M J_H(\vec{r'}) G_0(\vec{r}, \vec{r'}) d\vec{r'}, \vec{r} \in M \tag{2.7}$$

in H-polarization

where $\hat{n}$ is the outer normal, $J_{E,H}(\vec{r})$ are the unknown current densities, $G_0(\vec{r}, \vec{r'})$ is the 2-D Green's function (i.e $\frac{i}{4} H_0^{(1)}(k|\vec{r} - \vec{r'}|)$) and the contour M is taken as the surface of all the scatterers.

Equations (2.6) and (2.7) are widely known and can be solved numerically by the method of moments (MoM). Unfortunately MoM solutions lead to matrixes of great order N or increase the computation time due to massive numerical integration. In addition the problem often becomes ill-posed and does not guarantee convergence of the solution when $N \to \infty$. For these reasons, it is recommended to use other methods to calculate the radiated fields.

For our geometry the total field can be expressed as follows

$$U^{tot}\vec{r}) = \begin{cases} U^{inc}(\vec{r}) + U^{sc}(\vec{r}) & r < a \\ U^{sc}(\vec{r}) & r > a . \end{cases} \tag{2.8}$$

The scattered field satisfies the 2-D Helmholtz equation

$$(\nabla^2 + k_0^2) U^{sc}(\vec{r}) = 0. \tag{2.9}$$

Due to the axial symmetry of the problem it is expanded in series form as

$$U^{sc}(\vec{r}) = \sum_n \begin{cases} r_n J_n(k_0 r) e^{in\phi} & r < a \\ t_n H_n^{(1)}(k_0 r) e^{in\phi} & r > a . \end{cases} \tag{2.10}$$

where r_n and t_n are the unknown coefficients to be determined by the boundary conditions at $r = a$.

In region 1 ($r < a$) Bessel function is chosen to represent the standing wave nature of the scattered field, whereas in region 2 ($r > a$) Hankel function is chosen to satisfy the radiation condition at infinity.

Hence, the total field in region 1 is given by

$$U_1^{tot}(r, \phi) = \sum_n [C(J_n(k_0 r_s) H_n^{(1)}(k_0 r) e^{-in\theta_s} + r_n J_n(k_0 r)] e^{in\phi}, |r_s| < r < a \quad (2.11)$$

and in region 2 as

$$U_2^{tot}(r, \phi) = \sum_n t_n H_n^{(1)}(k_0 r) e^{in\phi} \quad (2.12)$$

2.2 General Form of Boundary Conditions

The boundary conditions to be used are established in [11] for the analysis of imperfectly conducting layers. We do realize that the set of boundary conditions available are valid for lossy materials, nevertheless the method can be generalized to quite good conductors. Actually, the concept of perfectly conducting material and of a perfectly conducting and infinitely thin screen is not always well understood [16]. For example, in the far infrared, gold is generally considered as infinitely conducting, however a very thin gold strip, like that found in telescopes, can be melted by a laser beam. Thus for practical purposes if a metal is supposed to have the same permittivity and permeability of free space and a real conductivity σ(a model often used in the far infra red and microwave ranges), it is equivalent to a lossy dielectric with relative permittivity $\epsilon_r = 1 + i\sigma/\epsilon_0\omega$.From now on, we consider imperfectly conducting metals.

The boundary conditions we shall be using are given in the following form

$$< E_T(r, \phi) >= R_T(r, \phi) J_T(r, \phi) \quad (2.13)$$

$$< H_T(r, \phi) >= S_T(r, \phi) M_T(r, \phi) \quad (2.14)$$

which relates the average tangential fields

$$< E_T(r, \phi) >= \frac{1}{2}[E_{2T}(r, \phi) + E_{1T}(r, \phi)] \qquad (2.15)$$

$$< H_T(r, \phi) >= \frac{1}{2}[H_{2T}(r, \phi) + H_{1T}(r, \phi)] \qquad (2.16)$$

to the currents defined by the field jumps

$$J_T(r, \phi) = \hat{n} \times [H_{2T}(r, \phi) - H_{1T}(r, \phi)] \qquad (2.17)$$

$$M_T(r, \phi) = -\hat{n} \times [E_{2T}(r, \phi) - E_{1T}(r, \phi)] \qquad (2.18)$$

Here the subscript 1 or 2 denotes the fields in respective regions, and R_T and S_T have the interpretation of the electric resistivity and magnetic conductivity of the interface separating regions 1 and 2. They can be regarded as phenomenological parameters which can be determined experimentally through the measurement of the reflection and transmission coefficients, or evaluated analytically according to [11].

An alternative version of this set of boundary conditions is written as

$$\hat{n} \times [H_{2T}(r, \phi) - H_{1T}(r, \phi)] = \xi_T(r, \phi)[E_{2T}(r, \phi) + E_{1T}(r, \phi)] \qquad (2.19)$$

$$- \hat{n} \times [E_{2T}(r, \phi) - E_{1T}(r, \phi)] = \eta_T(r, \phi)[H_{2T}(r, \phi) + H_{1T}(r, \phi)] \qquad (2.20)$$

where

$$\xi_T(r, \phi) = 1/(2R_T(r, \phi)) \qquad (2.21)$$

$$\eta_T(r, \phi) = 1/(2S_T(r, \phi)) \qquad (2.22)$$

Obviously, the boundary conditions have to be imposed on the strips. In our geometry, these strips form a periodic open contour, thus it is necessary for ξ_T and η_T to have a periodic step function of ϕ to account for the continuity of the total electric and magnetic fields at the slots (see Figure 2.3).

In the case of E polarization, (2.23) and (2.24) will be relating E_z and $H_\phi = \frac{i}{\omega\mu} \frac{\partial E_z}{\partial r}$ in the following way

$$H_{2\phi}(r, \phi) - H_{1\phi}(r, \phi) = \xi_T(r, \phi)[E_{2z}(r, \phi) + E_{1z}(r, \phi)]|_{r=a} \qquad (2.23)$$

$$E_{2z}(r, \phi) - E_{1z}(r, \phi) = \eta_T(r, \phi)[H_{2\phi}(r, \phi) + H_{1\phi}(r, \phi)]|_{r=a} \qquad (2.24)$$

with

$$\xi_T(\phi) = \begin{cases} \Delta & \text{if } \phi \in M \\ 0 & \text{if } \phi \in S \end{cases} \qquad (2.25)$$

$$\eta_T(\phi) = \begin{cases} \delta & \text{if } \phi \in M \\ 0 & \text{if } \phi \in S \ . \end{cases} \qquad (2.26)$$

Note that in the limit case $\Delta \to \infty$ and $\delta \to 0$ the boundary conditions reduce to the Dirichlet boundary condition for only perfectly conducting material $E_1 = E_2 = 0$.
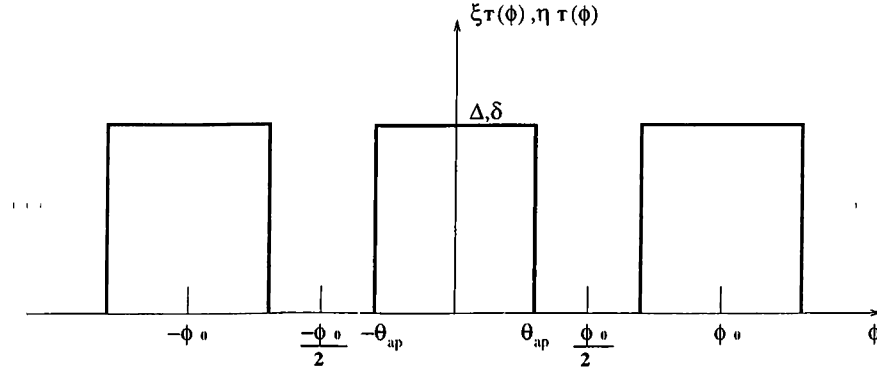

Figure 2.3: ξ_T and η_T functions of ϕ

2.3 Algebraic Solution of the Problem

To find the coefficients r_n and t_n it is convenient to write the functions $\xi_T(\phi)$ and $\eta_T(\phi)$ in their Fourier series expansion

$$\xi_T(\phi) = \sum_n \xi_{T_n} e^{inL\phi} \qquad (2.27)$$

and

$$\eta_T(\phi) = \sum_n \eta_{T_n} e^{inL\phi} \qquad (2.28)$$

where
$$\xi_{T_n},(\eta_{T_n}) = \Delta,(\delta)\begin{cases} 2\frac{\theta_{ap}}{\phi_0} & \text{if } n = 0 \\ \frac{1}{n\pi}sin(nL\theta_{ap}) & \text{if } n \neq 0 \end{cases}$$

and
$$L = \frac{2\pi}{\phi_0}.$$

Recalling that a periodic function f with period 2π and another g with period ϕ_0 where ϕ_0 divides 2π by an integer L are written as

$$f = \sum_n f_n e^{in\phi} \text{ and } g = \sum_n g_n e^{in\frac{2\pi}{\phi_0}\phi},$$

then their product $p = fg$ can be expanded in a generalized Fourier series

$$p = \sum_n p_n e^{in\phi} \text{with } p_n = \sum_m f_{n-mL}g_m$$

Therefore the expansion of (2.23) and (2.24) can be performed easily and we are led to

$$t_n x'_n + iZ_0 \sum_m \xi_{T_m} t_{n-mL} x_{n-mL} - r_n y'_n + iZ_0 \sum_m \xi_{T_m} r_{n-mL} y_{n-mL} =$$

$$z_n x'_n + iZ_0 \sum_m \xi_{T_m} z_{n-mL} x_{n-mL} \tag{2.29}$$

$$t_n x_n + \frac{1}{iZ_0} \sum_m \eta_{T_m} t_{n-mL} x'_{n-mL} - r_n y_n + \frac{1}{iZ_0} \sum_m \eta_{T_m} r_{n-mL} y'_{n-mL} =$$

$$z_n x_n + \frac{1}{iZ_0} \sum_m \eta_{T_m} z_{n-mL} x'_{n-mL} \tag{2.30}$$

where
$$\begin{aligned} x_n &= H_n^{(1)}(k_0 a) & x'_n &= H_n^{'(1)}(k_0 a) \\ y_n &= J_n^{(1)}(k_0 a) & y'_n &= J_n^{'(1)}(k_0 a) \\ & z_n = J_n(kr_s)e^{-in\theta_s} \end{aligned}$$

and Z_0:intrinsic impedance of free space .

Note that the derivatives are with respect to the argument. Keeping only $N_{tr} = 2N + 1$ terms in the Fourier series($n \leq N$), we get r_n and t_n by solving the system, and thus the fields in both regions.

The boundary conditions we have been using so far, rewritten here for convenience are

$$H_{2\phi} - H_{1\phi} = \xi_T(E_{2z} + E_{1z}) \tag{2.31}$$

$$E_{2z} - E_{1z} = \eta_T(H_{2\phi} + H_{1\phi}). \tag{2.32}$$

By setting $\eta_T = 0, \xi_T \neq 0$ we obtain the well known set of equations for a thin dielectric resistive sheet (i.e a sheet of high conductivity and its resistivity is small compared to free space impedance)

$$H_{2\phi} - H_{1\phi} = \xi_T(E_{2z} + E_{1z}) \tag{2.33}$$

$$E_{2z} = E_{1z}. \tag{2.34}$$

With these two equations we can solve for r_n and t_n independently. The field of interest is the one at the far zone which includes t_n. We obtained the following equation in t_n

$$\frac{x'_n y_n - x_n y'_n}{y_n} t_n + 2iZ_0 \sum_m \xi_{T_n} x_{n-mL} t_{n-mL} = \frac{x'_n y_n - x_n y'_n}{y_n} z_n \tag{2.35}$$

where x_n, y_n, x'_n, y'_n and z_n are as the ones used in (2.29) and (2.30).

2.4 Radiation Through A Radome of Periodic Metal-Dielectric Grating

Previously, we have considered the problem of thin periodic metal grating. The strips are modeled as infinitely thin structures described in terms of a set of boundary conditions relating the fields from the interior and exterior sides by the two coefficients R_T and S_T (2.13 and 2.14) known as electric resistivity and magnetic conductivity respectively. While treating thin structures, it is convenient to define real constant resistivities and conductivities for the strips, however for a layer of finite thickness, this assumption does not hold because these coefficients depend on the microscopic properties and thickness of the layer.

For a dielectric/magnetic layer characterized by material parameters ϵ, μ and thickness h, the respective values of R_T and S_T are

$$R_T = \frac{i}{2}\sqrt{\frac{\mu}{\epsilon}}\cot\left(\frac{1}{2}\sqrt{\frac{\epsilon\mu}{\epsilon_0\mu_0}}k_0 h\right) \tag{2.36}$$

$$S_T = \frac{i}{2}\sqrt{\frac{\epsilon}{\mu}}\cot\left(\frac{1}{2}\sqrt{\frac{\epsilon\mu}{\epsilon_0\mu_0}}k_0 h\right) \tag{2.37}$$

which can be written as

$$R_T = \frac{i}{2}Z\cot\left(k\frac{h}{2}\right) \tag{2.38}$$

$$S_T = \frac{i}{2}\frac{1}{Z}\cot\left(k\frac{h}{2}\right) \tag{2.39}$$

where

$$Z = Z_0/\sqrt{\hat{\epsilon}_r}$$
$$k = k_0\sqrt{\hat{\epsilon}_r}$$
$$\hat{\epsilon}_r = \epsilon_r + i\frac{\sigma}{\omega\epsilon_0}$$

Surely the use of these values for the parameters R_T and S_T have practical advantages such as the choice of the metal strips characteristics and thickness. Also, we can now insert dielectric between the strips (see Figure 2.4). This will enable us to investigate the effect of a circular dielectric radome with metal grating, which is the aim of this thesis.

The formulation of the problem for such geometry is carried out exactly as that for thin metal gratings, except that $\xi_T = 1/(2R_t)$ and $\eta_T = 1/(2S_T)$ will have a different function of ϕ from that of Figure 2.3. In this case ξ_T and η_T are now a periodic function of ϕ as shown in Figure 2.5

The Fourier series coefficients ξ_{T_n}'s are given as

$$\xi_{T_n} = \begin{cases} (\Delta_m - \Delta_s)2\frac{\theta_{ap}}{\phi_0} + \Delta_s & \text{if } n = 0 \\ (\Delta_m - \Delta_s)\frac{1}{n\pi}sin(nL\theta_{ap}) & \text{if } n \neq 0 \end{cases} \tag{2.40}$$
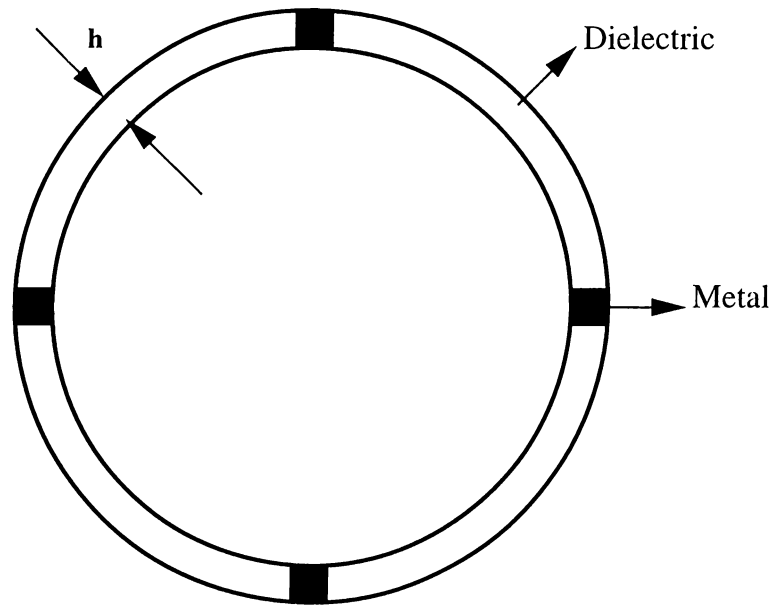
and the coefficients η_{T_n}'s as

$$\eta_{T_n} = \begin{cases} (\delta_m - \delta_s)2\frac{\theta_{ap}}{\phi_0} + \delta_s & \text{if } n = 0 \\ (\delta_m - \delta_s)\frac{1}{n\pi}sin(nL0_{ap}) & \text{if } n \neq 0 \end{cases} \qquad (2.41)$$

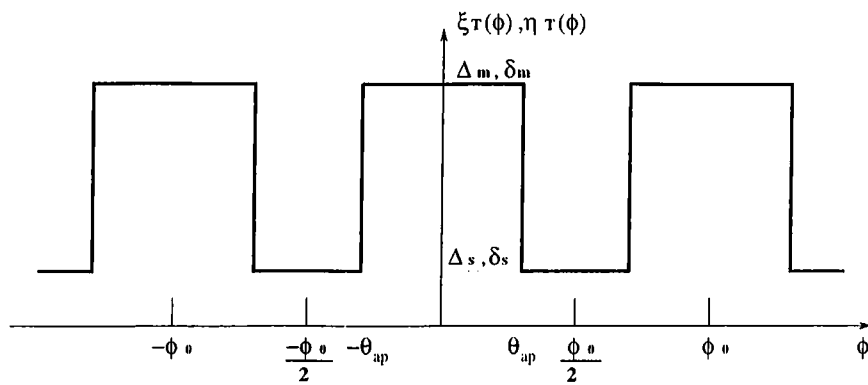Figure 2.4: Geometry of a circular radome with periodic metal gratings

Figure 2.5: ξ_T and η_T functions of ϕ
(the plot is understood for either real or imaginary parts of the functions).

Chapter 3

NUMERICAL RESULTS AND DISCUSSION

As mentioned in the introduction, the aim of this study is to analyze the effect of a metal-dielectric periodic radome on the transmission of electromagnetic fields radiated by a complex line source placed inside this structure. The subject is discussed in terms of normalized power at the far zone and the directivity, which represent two important parameters in design problems. The associated formula for the normalized power pattern is given as

$$P_{Norm} = \frac{|\, E_2^{tot}(r, \phi)\,|^2}{|\, E_2^{max}(r, \phi)\,|^2} \tag{3.1}$$

For far field observation ($kr \gg 1$) the total electric field can be reduced by replacing the Hankel function $H_n^{(1)}(k_0 r)$ by its asymptotic expression. By doing this we obtain

$$E_2^{tot}(r, \phi) = \sqrt{\frac{2}{i\pi K_0}} \frac{e^{ik_0 r}}{\sqrt{r}} \sum_n (-i)^n t_n e^{in\phi} \tag{3.2}$$

16

which is more convenient for numerical computations.

The directivity, which is the ratio of the maximum radiation intensity to the average radiation intensity, in terms of electric field intensity is given by

$$D = \frac{2\pi \mid E_2^{max} \mid^2}{\int_0^{2\pi} \mid E_2(\phi) \mid^2 d\phi}. \tag{3.3}$$

Using Parseval's Relation

$$\frac{1}{T_0} \int_{T_0} \mid x(t) \mid^2 dt = \sum_k \mid a_k \mid^2, \tag{3.4}$$

D can be expressed as

$$D = \frac{\mid E^{max} \mid^2}{\sum_n \mid t_n \mid^2}. \tag{3.5}$$

In the formulation of the problem, it is stated that exact solutions are not available and are not obtained easily due to several reasons, so approximations have been used to establish the outer fields due to the source enclosed by the radome. The basic approximation employed is to model the radome as thin layer described by means of boundary conditions. The set of boundary conditions provided, relate the inner electric and magnetic fields to the outer ones through two coefficients evaluated by the structure and the material properties of the the layer representing the radome. This approach as already mentioned considers non perfect metals.

In our investigation, attention was focused on periodic metal gratings since they are strong scatterers compared to dielectrics, especially when the dielectric thickness is half the wave length. Thus metal grating are of primary importance for the scattered fields. In this chapter, the numerical results for two different models of the radome are obtained. The first model is described by thin periodic

metal gratings surrounded by vacuum, whereas the second model represents a dielectric radome with periodic metal gratings. For the first model results are given at two levels. Due to high conductivity, resistive boundary conditions are used to obtain the results for the far field patterns. This simplified boundary condition assumes the continuity of the electric field through the metal strips. This is due mainly to the fact that the electric field is almost zero on the metal interface so it is considered to be equal at the two faces. This assumption has been widely used in scattering from resistive layers and the boundary conditions are often referred as transparency boundary conditions. Then the general boundary conditions are used to show the limitations of the former ones.

3.1   Radomes of Periodic Metal Gratings

In Figure (3.1), the normalized power at the far zone for a circular reflector antenna is obtained(only one strip). This result coincides exactly with the one obtained by solving the integral equations (IE) corresponding to such a geometry [17]. This is expected because our rigorous solution of the problem is in fact the same as IE solutions. For a non PEC, in the case of E-pol the scattered field is expressed in integral form as

$$\int J_T(\vec{r})G(\vec{r},\vec{r'})d\vec{r'} = -E_z^{inc}(\vec{r}) + RJ_T(\vec{r}) \qquad (3.6)$$

where J_T is the unknown surface current and R is the effective resistance of the scatterer.

In our formulation the scattered field is written in series expansion with unknown coefficients which are determined by imposing the boundary conditions and we were led to solve the following equation.

$$E_z^{inc} + \sum_n r_n H_n(k_0 r)e^{in\phi} = RJ_T(r)|_{r=a} \qquad (3.7)$$

which is equivalent to (3.6) except that the scattered field is expressed in series expansion with separate variables, rather than the compact integral form.

Knowing that our results show good agreement with IE solutions for the case of a reflector antenna, further numerical data for other geometries are obtained.

The normalized power for two circular opposite reflectors is shown in Figure (3.2). The reflectors have the same dimensions as the used to obtain Figure (3.1). The source has the same location and direction as well. A drop in the power is observed at $\phi = 180°$, compared to Figure (3.1).This behavior is understandable due to the presence of the second reflector at that position.

In Figures (3.3) through (3.6) the normalized power at the far zone for gratings consisting of a periodic array of two, three, four and five strips is obtained for different angular widths when $ka = 62.8$, $r_0 = 0$, $kb = 5$ (Beam Width= $42°$)and $\beta = 0$. The ratio of the strip resistivity to free space impedance is taken as $2R_T/Z_0 = 0.1\%$. The same results are obtained for more resistive strips, $2R_T/Z_0 = 10\%$ (Figures (3.7) to (3.10)). As observed in these figures, the distortion of the main beam increases with increasing number of strips which is mainly due to the contribution of each strip to the scattered fields as expected. Increasing the angular width of the strips also increases beam distortion and causes a shift in the main beam direction. It is noticed that increasing the resistivity reduces the boresight error (the difference between the apparent and the distorted beam direction). For strips with $2R_T/Z_0 = 0.1\%$ and $2R_T/Z_0 = 10\%$, the shift in the main beam direction occurs at an angular width of $2°$ whereas this behavior appears at an angular width of $3°$ for strips of higher resistivity ($2R_T/Z_0 = 10\%$) and in general the patterns are quite similar for these two cases. This shows that good conductors have greater effect on the distortion of fields which is reasonable since they are stronger scatterers. Another point worth mentioning is that through all these figures, the power at $\phi = 180°$ (opposite to the main beam direction) increases as the angular width increases.
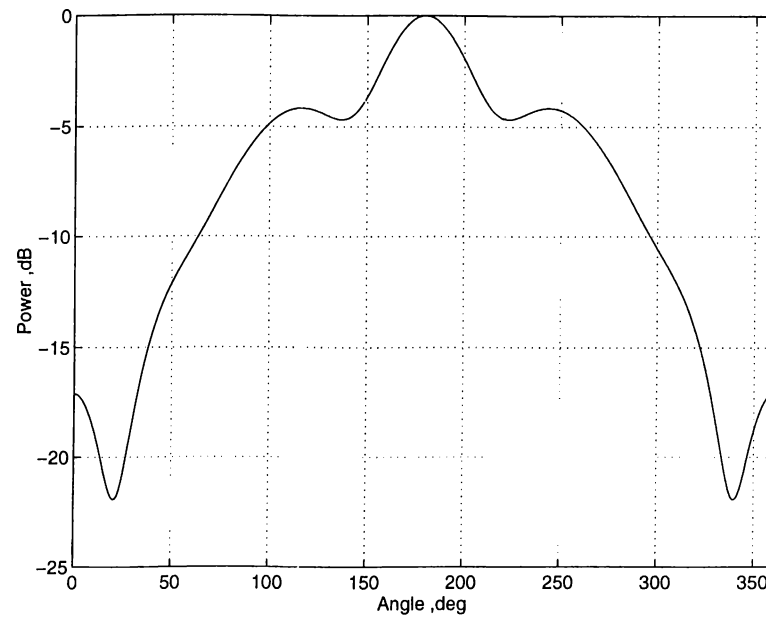
Figure 3.1: Normalized power at the far zone for a circular reflector antenna: $2R_T/Z_0 = 5 \times 10^{-5}$, $ka = 6.28, r_0 = a/2, \beta = 0, \theta_{ap} = 30$ degrees, $kb = 0.5$.
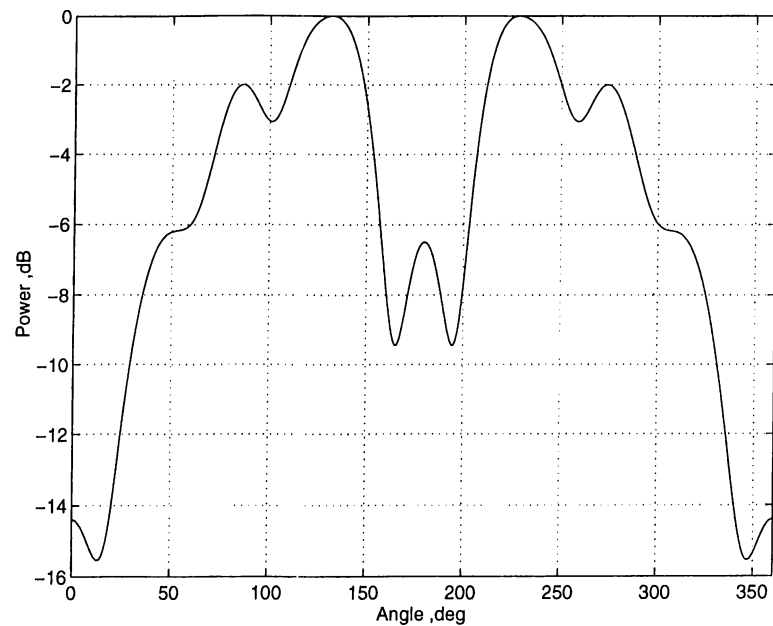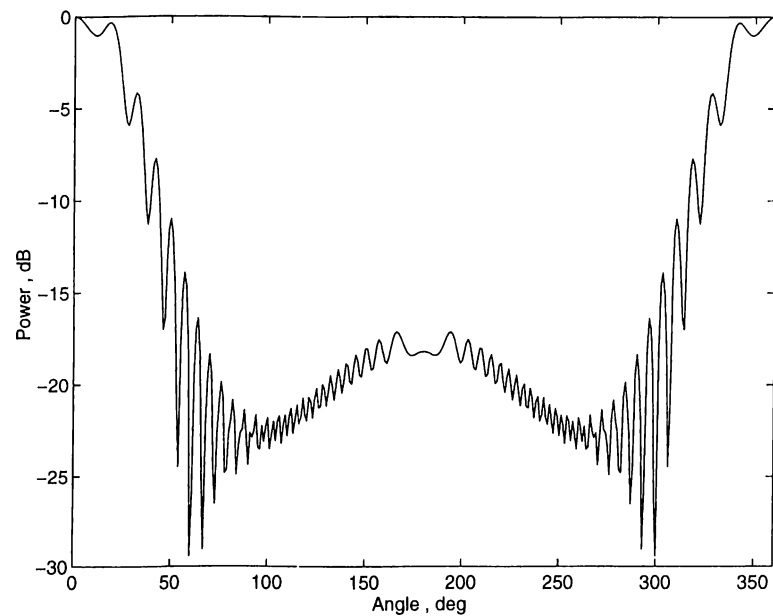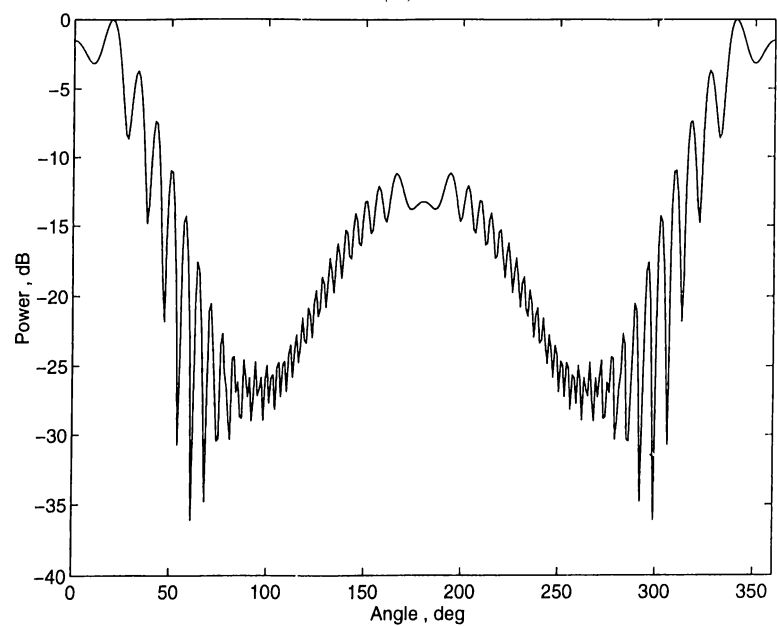

Figure 3.2: Normalized power at the far zone for 2 circular opposite strips: $2R_T/Z_0 = 5 \times 10^{-5}$, $ka = 6.28, r_0 = a/2, \beta = 0, \theta_{ap} = 30$ degrees, $kb = 0.5$.
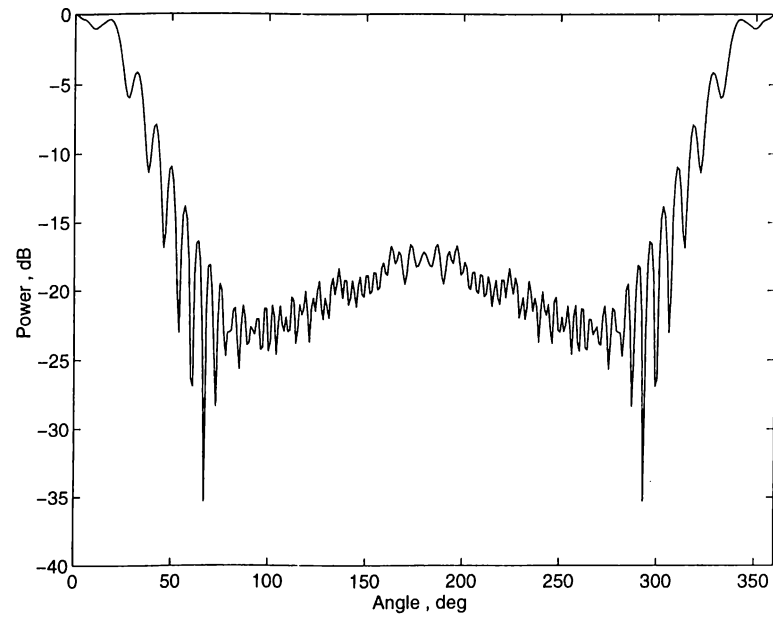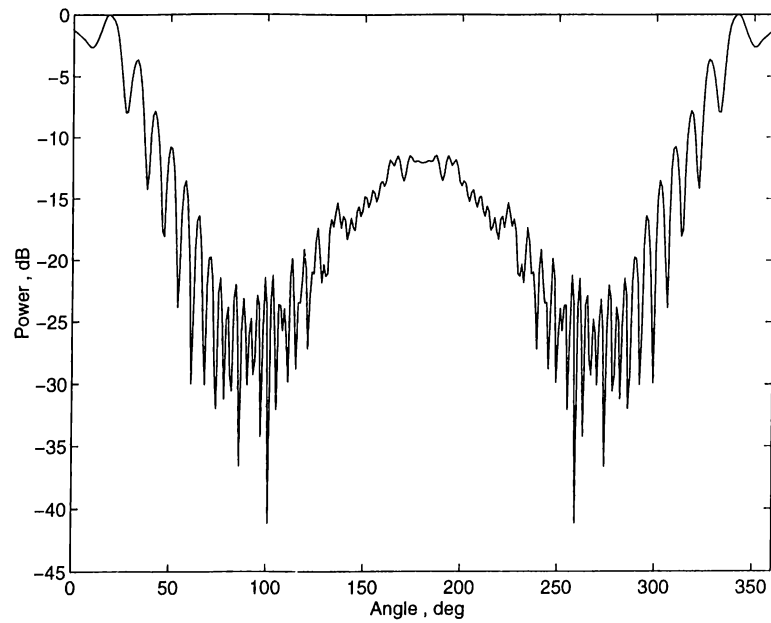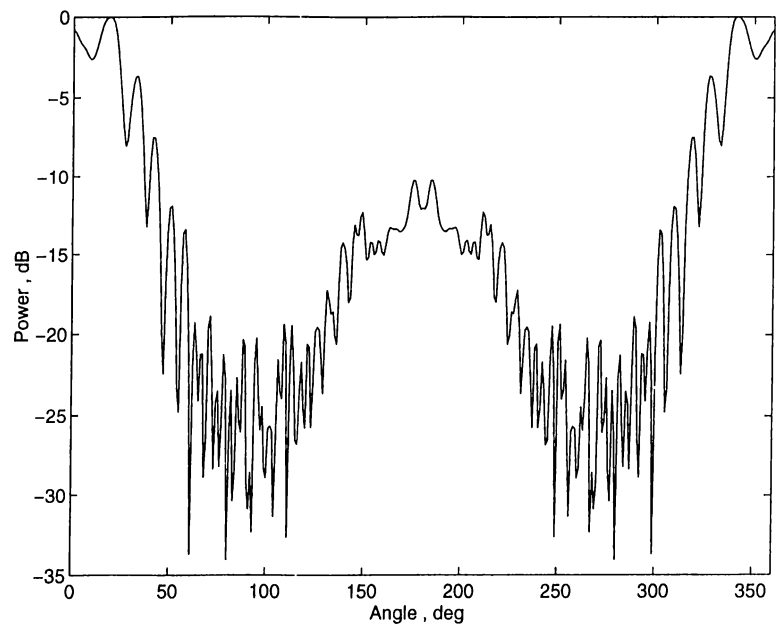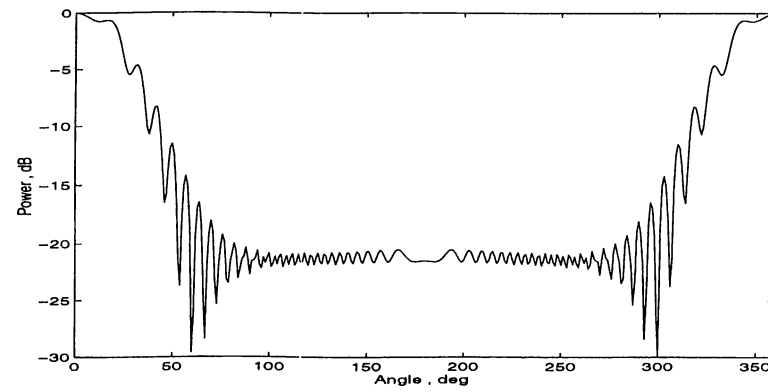
(a)

(b)

Figure 3.3: Normalized power at the far zone for a grating consisting of two resistive strips : $ka = 62.8$, $kb = 5$, $\beta = 0°$, $2R_T/Z_0 = 0.1\%$, (a) $\theta_{ap} = 0.5°$, (b) $\theta_{ap} = 1°$.
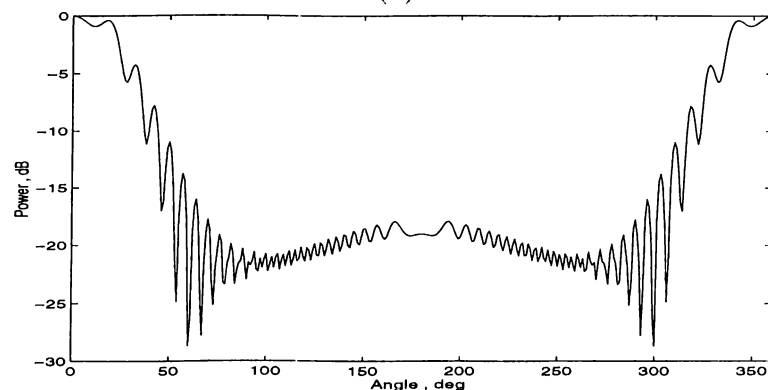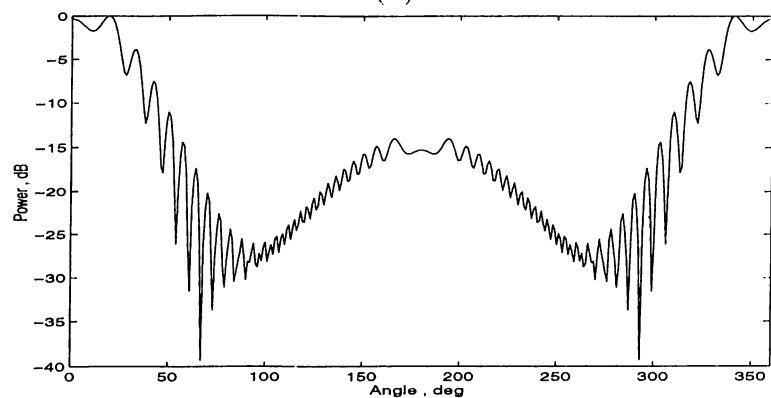
(a)

(b)

Figure 3.4: Normalized power at the far zone for a grating consisting of three resistive strips : $ka = 62.8$, $kb = 5$, $\beta = 0°$, $2R_T/Z_0 = 0.1\%$, (a) $\theta_{ap} = 0.5°$, (b) $\theta_{ap} = 1°$.
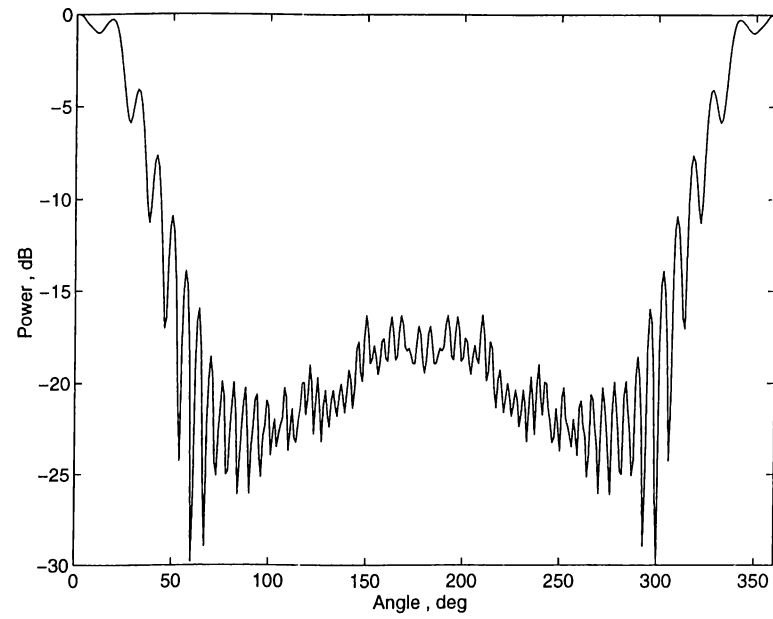
(a)
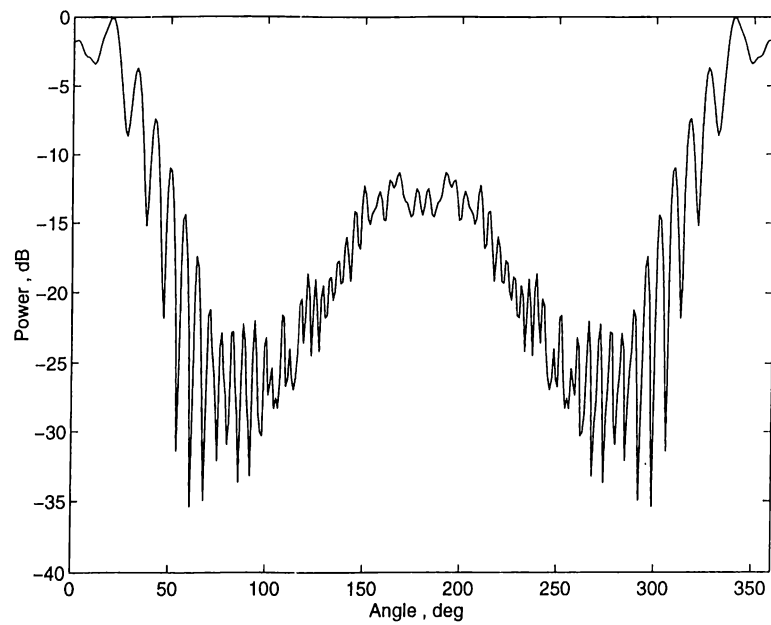
(b)

Figure 3.5: Normalized power at the far zone for a grating consisting of four resistive strips : $ka = 62.8$, $kb = 5$, $\beta = 0°$, $2R_T/Z_0 = 0.1\%$, (a) $\theta_{ap} = 0.5°$, (b) $\theta_{ap} = 1°$.
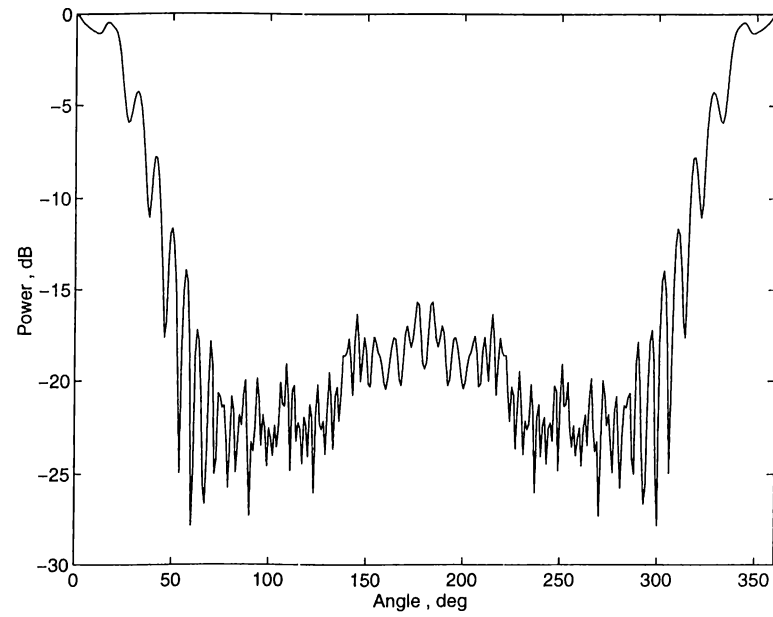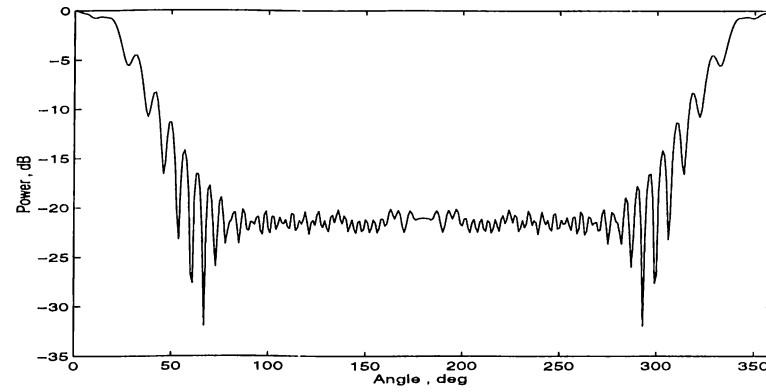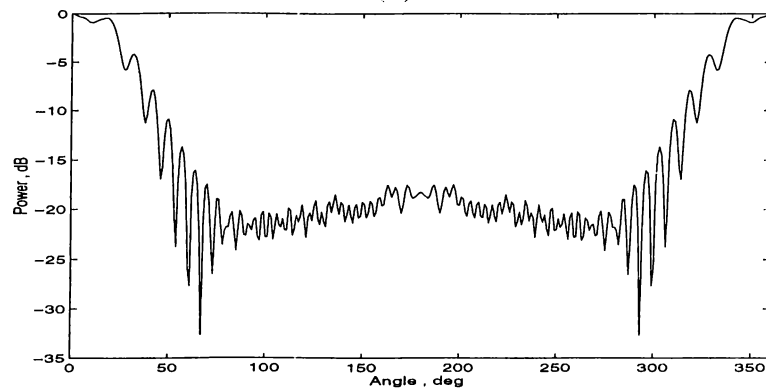
(a)

(b)

Figure 3.6: Normalized power at the far zone for a grating consisting of five resistive strips : $ka = 62.8$, $kb = 5$, $\beta = 0°$, $2R_T/Z_0 = 0.1\%$, (a) $\theta_{ap} = 0.5°$, (b) $\theta_{ap} = 1°$.
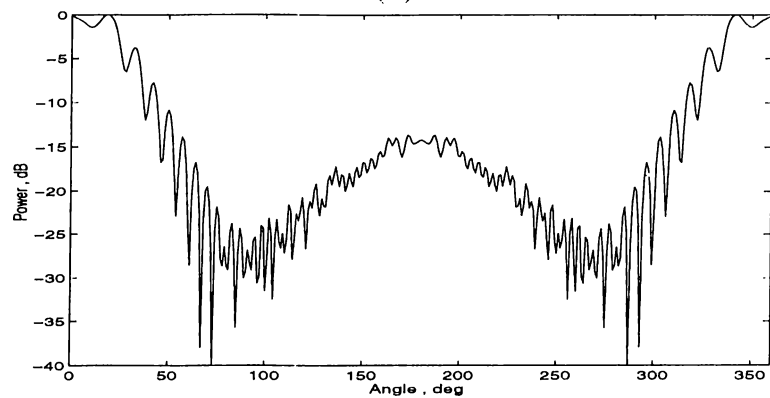
(a)

(b)

(c)

Figure 3.7: Normalized power at the far zone for a grating consisting of two resistive strips : $ka = 62.8$, $kb = 5$, $\beta = 0°$, $2R_T/Z_0 = 10\%$, (a) $\theta_{ap} = 0.5°$, (b) $\theta_{ap} = 1°$, (c) $\theta_{ap} = 1.5°$.
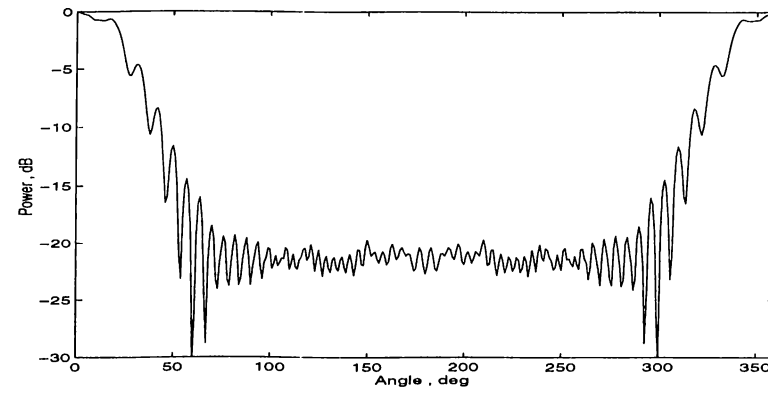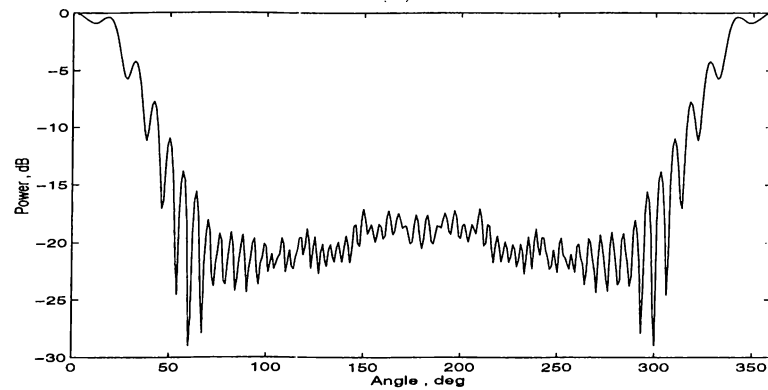
(a)

(b)

(c)

Figure 3.8: Normalized power at the far zone for a grating consisting of three resistive strips : $ka = 62.8$, $kb = 5$, $\beta = 0°$, $2R_T/Z_0 = 10\%$, (a) $\theta_{ap} = 0.5°$, (b) $\theta_{ap} = 1°$, (c) $\theta_{ap} = 1.5°$.

Figure 3.9: Normalized power at the far zone for a grating consisting of four resistive strips: $ka = 62.8$, $kb = 5$, $\beta = 0°$, $2R_T/Z_0 = 10\%$, (a) $\theta_{ap} = 0.5°$, (b) $\theta_{ap} = 1°$, (c) $\theta_{ap} = 1.5°$.
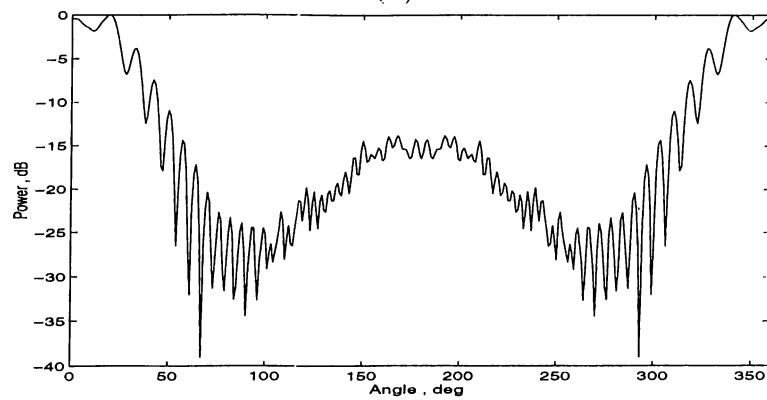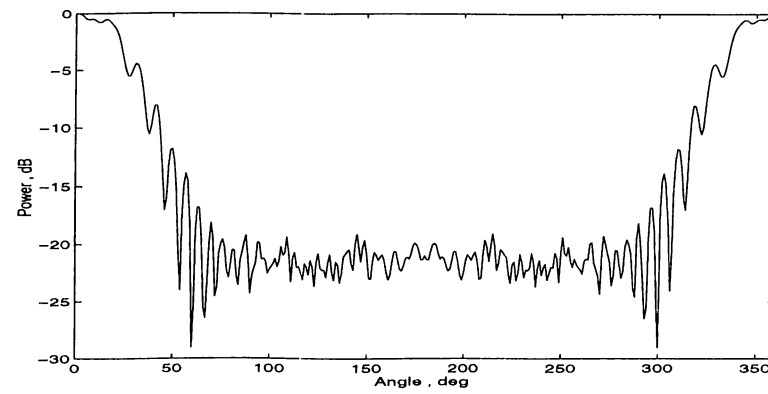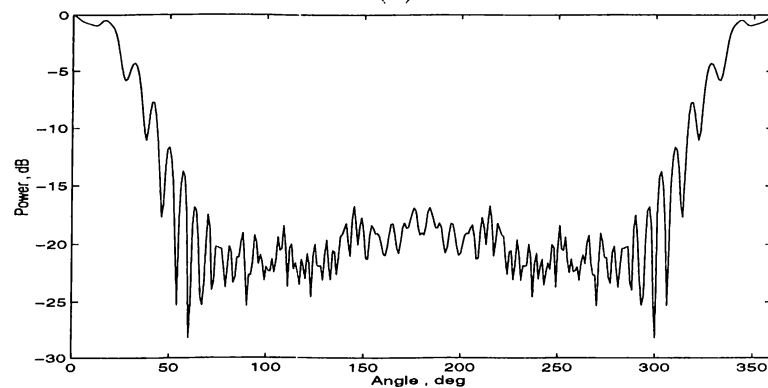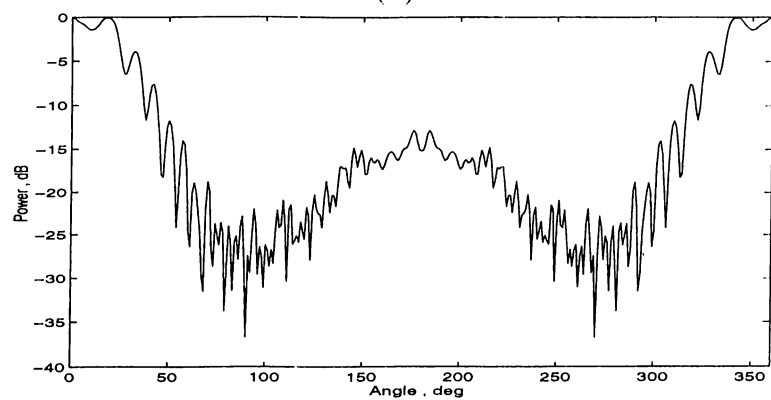
(a)

(b)

(c)

Figure 3.10: Normalized power at the far zone for a grating consisting of five resistive strips : $ka = 62.8$, $kb = 5$, $\beta = 0°$, $2R_T/Z_0 = 10\%$, (a) $\theta_{ap} = 0.5°$, (b) $\theta_{ap} = 1°$, (c) $\theta_{ap} = 1.5°$.

After analyzing the far-zone normalized power for different geometries, the directivity, which is a commonly used parameter to measure the overall ability of an antenna to direct radiated power, will be discussed. Figures (3.11),(3.12)and (3.13) present the variations of the overall directivity D with angular width for periodic gratings of various number of strips with different resistivities. As expected increasing the angular width decreases the directivity. However some weak resonant behavior which is related to the strip width values, around approximately integer multiple of $\lambda/2$, is observable. Throughout these three figures, the number of strips does not affect the directivity up to a critical angular width, related to the linear width of the strip $d \approx \lambda/2$(if $d = \lambda/2$, $\theta_{ap} = 1.4°$, after which the difference becomes more observable. It is found that, at this width the boresight error starts to increase considerably. As observed in these figures that this critical angular width becomes wider as the resistivity of the strips increases. It is of 0.8° for materials of resistivity $2R_T/Z_0 = 0.1\%$, 1.5° for $2R_T/Z_0 = 1\%$, and 2° for $2R_T/Z_0 = 10\%$. The directivity at these points is higher as the resistivity decreases. For good conductors (Fig 3.13), we see that the directivity drops sharply just after zero width and then it keeps nearly constant value up to the critical width, while it decreases at a lower rate for more resistive materials.

We notice as well that gratings consisting of periodic arrays of two and four strips show very close behavior; however, for gratings of three and five strips the results differ from each other. Similarities appear for two and four strips due to the symmetric structure of the geometry. In addition the beam is directed to the strip and narrow enough that it does not affect the the strips at $\phi = \pm90°$.

The directivity variations versus the beam direction are presented in Figures (3.14) through (3.17) for gratings of two, three four and five strips when $ka = 62.8$, $r_0 = 0$, $kb = 5$ and $\theta_{ap} = 1°$. The data are obtained for two different resistivities of the strips ($2R_T/Z_0 = 1\%$ and $2R_T/Z_0 = 10\%$). Again, we see that the directivity decreases with increasing resistivity which shows good agreement with the previous results.
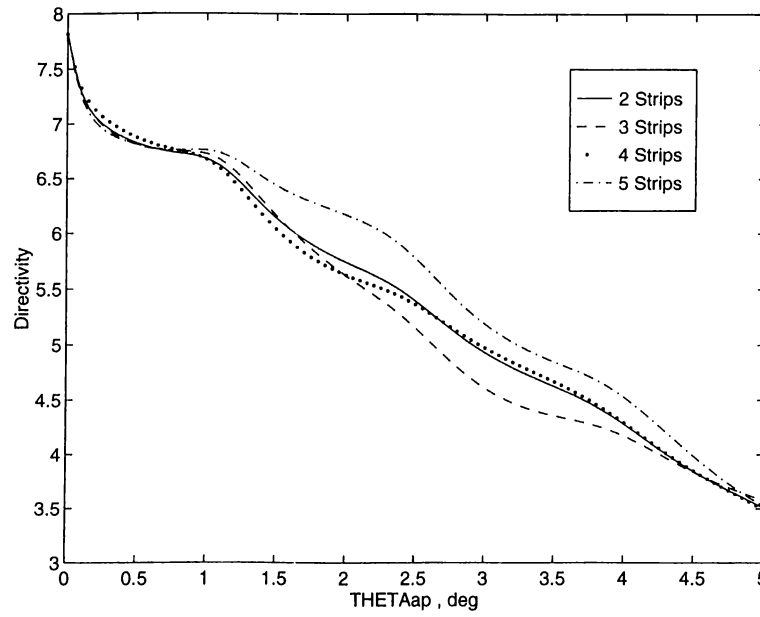
Figure 3.11: Directivity versus Angular Width of Strips (θ_{ap}) : $ka = 62.8$, $kb = 5$, $\beta = 0°$, $2R_T/Z_0 = 10\%$.
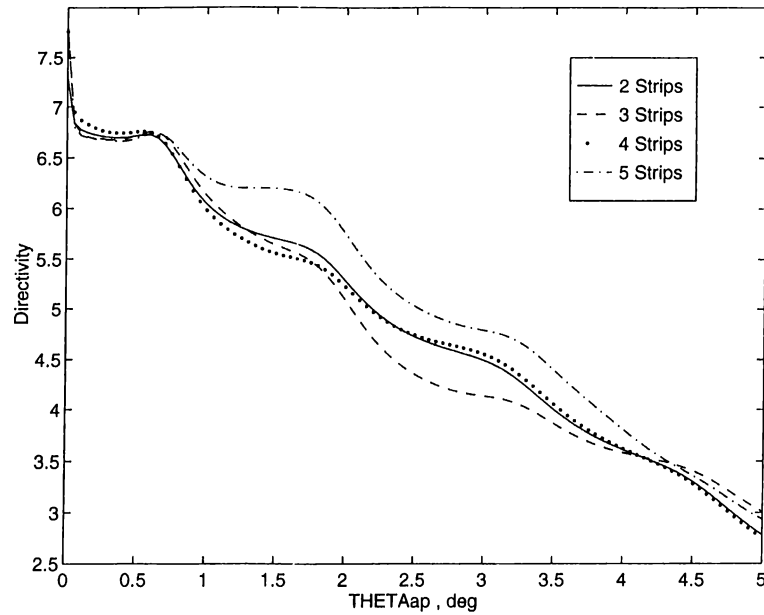

Figure 3.12: Directivity versus Angular Width of Strips (θ_{ap}) : $ka = 62.8$, $kb = 5$, $\beta = 0°$, $2R_T/Z_0 = 1\%$.
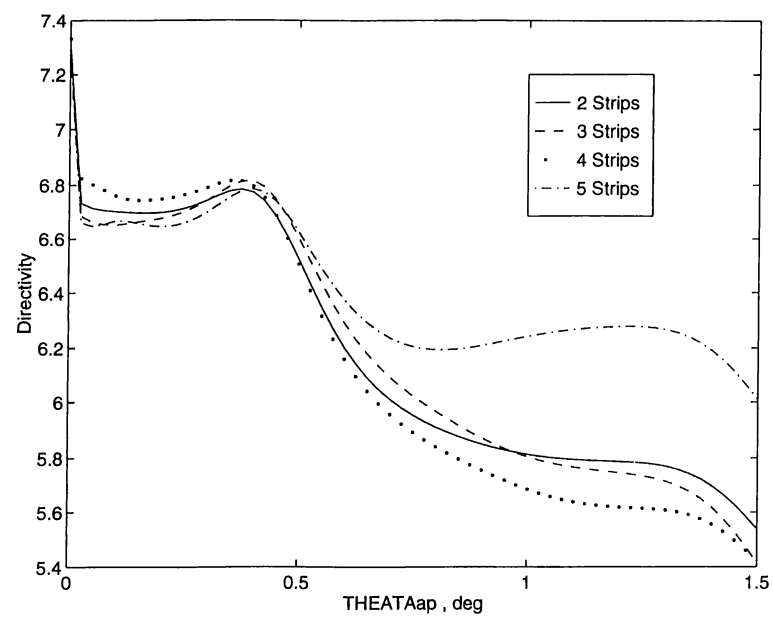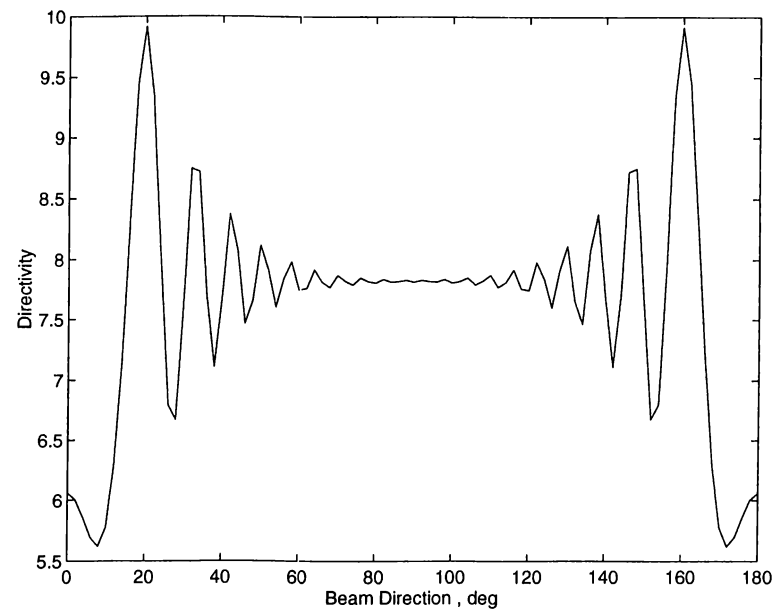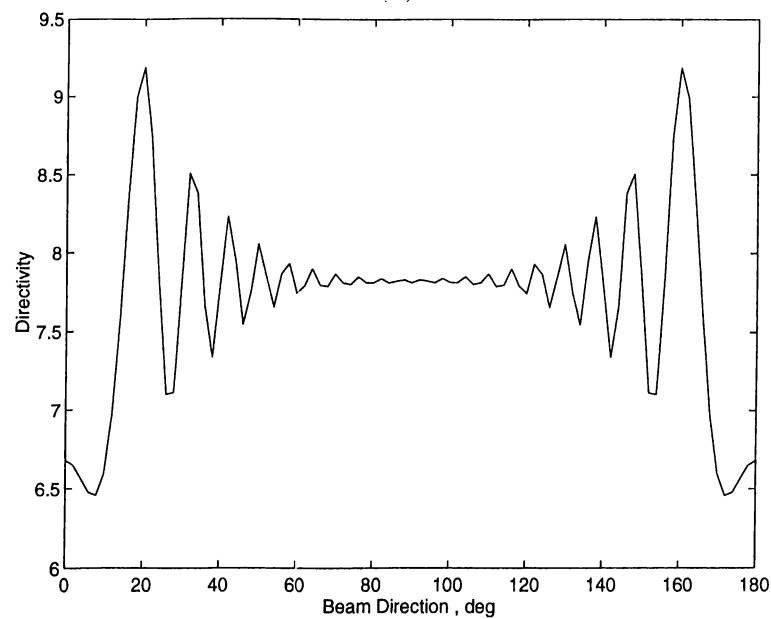
Figure 3.13: Directivity versus Angular Width of Strips (θ_{ap}) : $ka = 62.8$, $kb = 5$, $\beta = 0°$, $2R_T/Z_0 = 0.1\%$.

(a)

(b)

Figure 3.14: Directivity versus Beam Direction for a grating consisting of two resistive strips : $ka = 62.8$, $kb = 5$, $\theta_{ap} = 1°$, (a) $2R_T/Z_0 = 1\%$, (b) $2R_T/Z_0 = 10\%$.

(a)

(b)

Figure 3.15: Directivity versus Beam Direction for a grating consisting of three resistive strips : $ka = 62.8$, $kb = 5$, $\theta_{ap} = 1°$, (a) $2R_T/Z_0 = 1\%$, (b) $2R_T/Z_0 = 10\%$.

(a)

(b)

Figure 3.16: Directivity versus Beam Direction for a grating consisting of four resistive strips : $ka = 62.8$, $kb = 5$, $\theta_{ap} = 1°$, (a) $2R_T/Z_0 = 1\%$, (b) $2R_T/Z_0 = 10\%$.
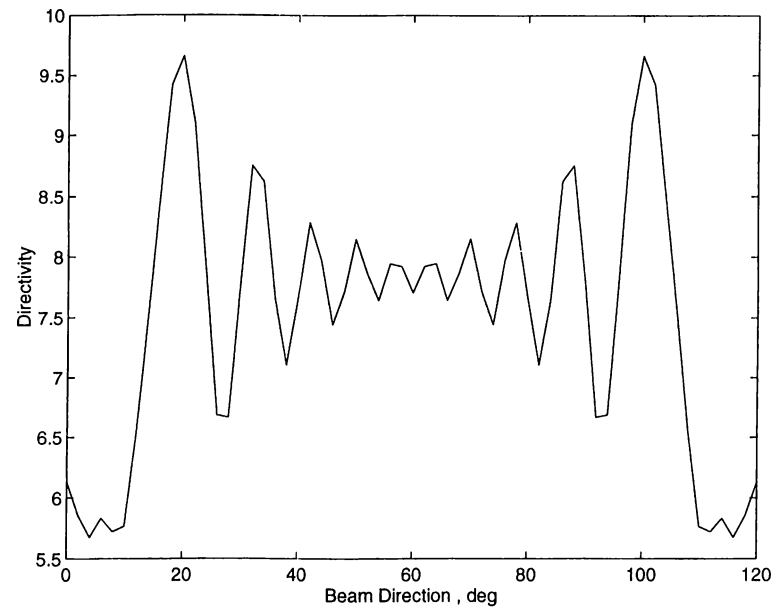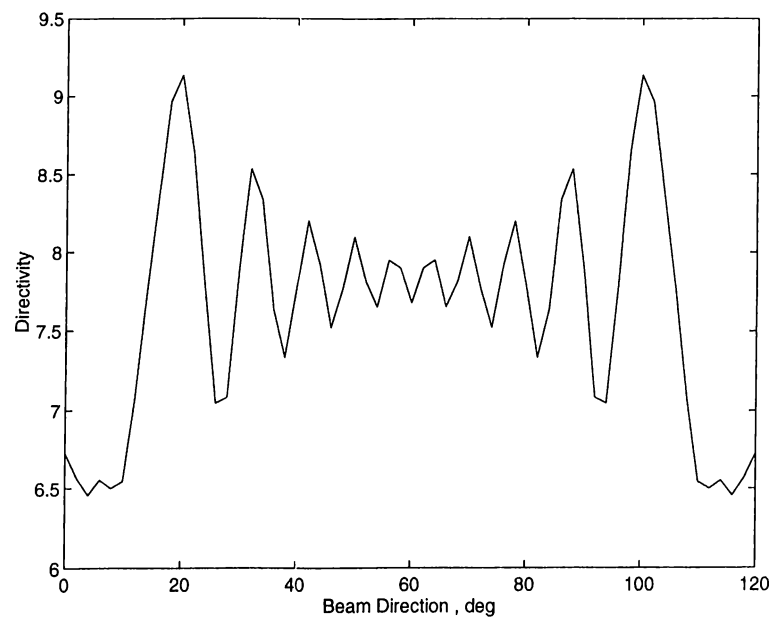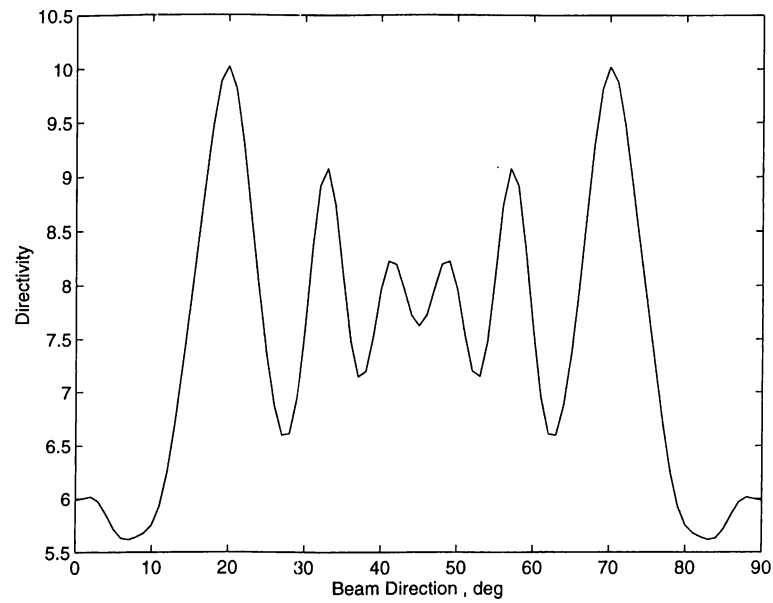
(a)
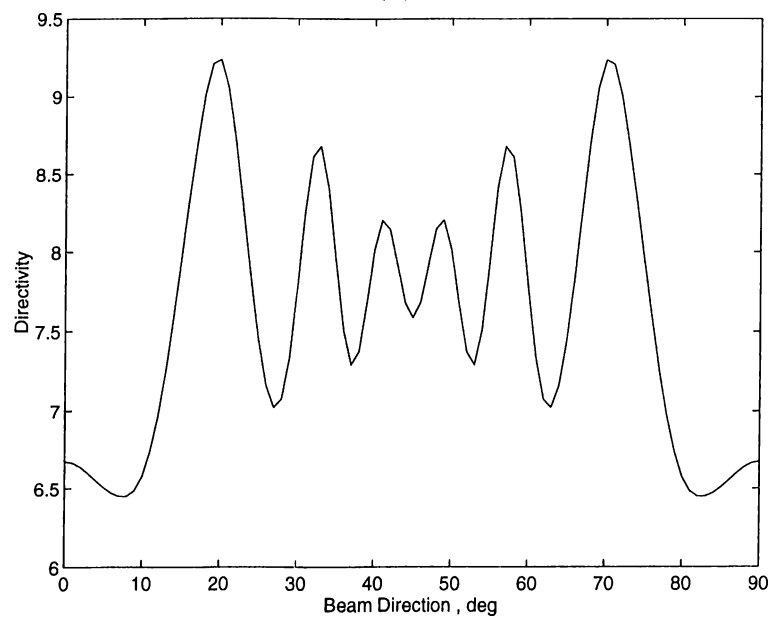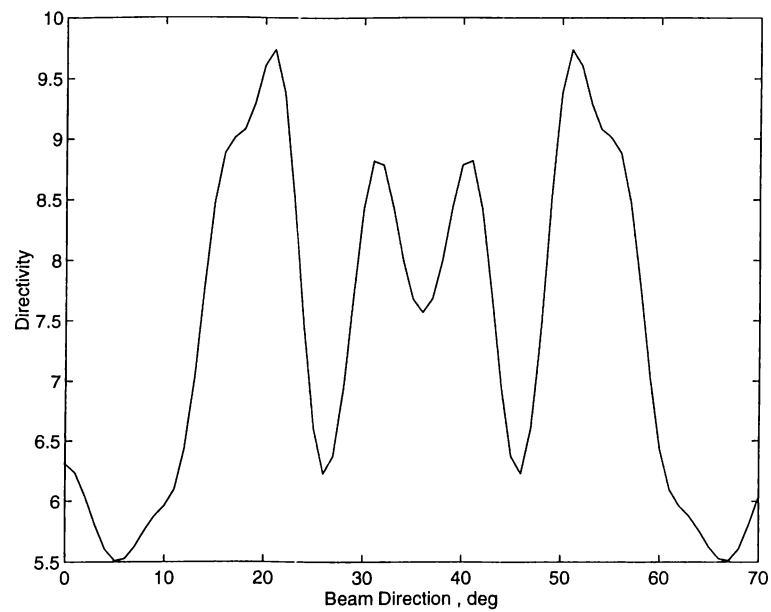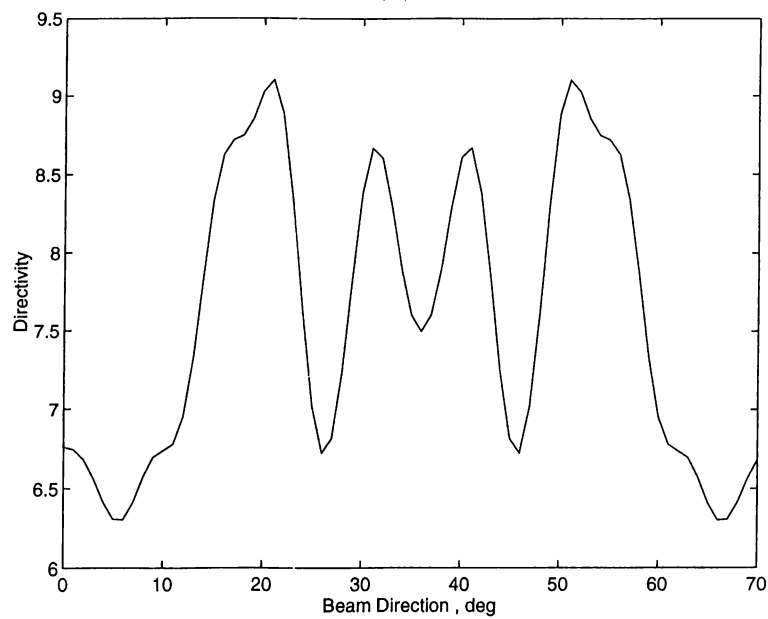

(b)

Figure 3.17: Directivity versus Beam Direction for a grating consisting of five resistive strips : $ka = 62.8$, $kb = 5$, $\theta_{ap} = 1°$, (a) $2R_T/Z_0 = 1\%$, (b) $2R_T/Z_0 = 10\%$.

3.2 Radomes of Periodic Metal-Dielectric Grating

The results we have discussed previously were obtained using the simplified version of boundary conditions valid for thin dielectric layers. As stated in the beginning of this chapter, these boundary conditions have been widely employed in scattering problems for electrically resistive sheets. However, they become inapplicable to magnetically conductive strips or sheets of non-zero thickness. In Figure (3.18) we have plotted again the far-zone normalized power for a circular reflector antenna with the same dimensions and parameters like in Figure (3.1). In this case we set $S_T = S \neq \infty$. The patterns coincide with the one presented in Figure (3.1) when S_T is large compared to $Y_0 = 1/Z_0$, but when we decrease the magnetic conductivity S_T, the results deviate from the initial one and we start loosing accuracy. Thus, the method of using transparency boundary conditions is not valid anymore. To show the limitations of this method , we have obtained the directivity variations versus thickness for a circular dielectric radome when $ka = 62.8$ $r_0 = 0$, $kb = 5$ and $\beta = 0$ using the simplified and generalized boundary conditions. The periodicity of the directivity as a function of thickness is observed, with period $\lambda_{diel}/2$ as expected when the generalized boundary conditions are applied, whereas incorrect periodicity is obtained with simplified boundary conditions(see Figure 3.19). The values of the directivity calculated by the two methods are close to each other just for very small thickness ($< 0.2\lambda_{diel}$) which proves that the simplified boundary conditions are valid only for thin electrically resistive sheets.

In Figures(3.20) to (3.23) the directivity versus thickness is obtained for a circular dielectric radome for different source directivities using the generalized boundary conditions. For the validation of the results, we have checked the exact solution [8] for the same geometry with the same dimensions and parameters. As observed in these figures, our results show good agreement with the exact ones. The difference between the two solutions increases as the source directivity increases, but this appears only at the minimum values of the directivities, which is not very important since in design problems high directivity is desired.

Further results for the directivity are obtained for a circular metal-dielectric radome with four metal strips when $ka = 62.8, kr_0 = 0$ and $kb = 5$. Figure (3.24) shows the directivity variations with increasing dielectric thickness for three beam directions. The metal strips have angular width $2\theta_{ap} = 1°$ and relative resistivity $2R_T/Z_0 = 1\%$. The dielectric is perfect with $\tilde{\epsilon}_r = 4$. It is seen that the directivity for the three orientations of the source converge to the same value which is close to the free space directivity when the thickness of the dielectric is an odd multiple of $\lambda_{diel}/2$. This behavior is desirable for radome construction around a radar antenna.

In Figure (3.25) the directivity versus the angular width of the metal strips presented. It is observed that the variations are less sensitive to the width and the beam direction when perfect dielectric is used with narrow strips. To look for the limiting values of the strip width and the perfectness of the dielectric, directivity variations function of the beam direction are plotted in Figures (3.26) through (3.28) for radomes consisting of metal gratings in free space, lossy dielectric-metal and perfect dielectric radomes.

As observed in these figures, the insertion of a dielectric layer between the metal strips decreases the directivity variations as compared with metal in vacuum. The directivity is nearly constant when perfect dielectric is used. However, this is not valid for all widths of the metal strips. When the angular width increases, the variations in the directivity become more considerable and tend the case of metal gratings surrounded free space.
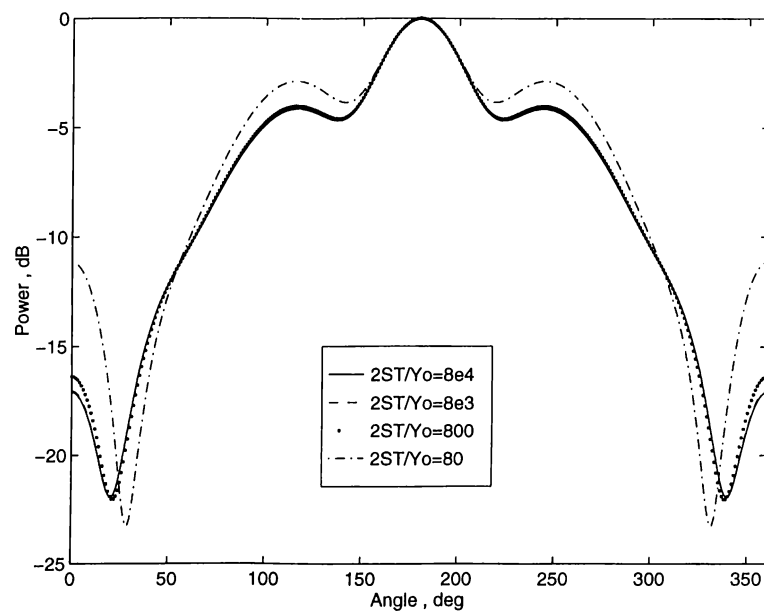
Figure 3.18: Normalized Power at the far zone for circular reflector antenna: $2R_T/Z_0 = 5 \times 10^{-5}$, $ka = 6.28$, $r_0 = a/2$, $\beta = 0$, $\theta_{ap} = 30°$, $kb = 0.5$.
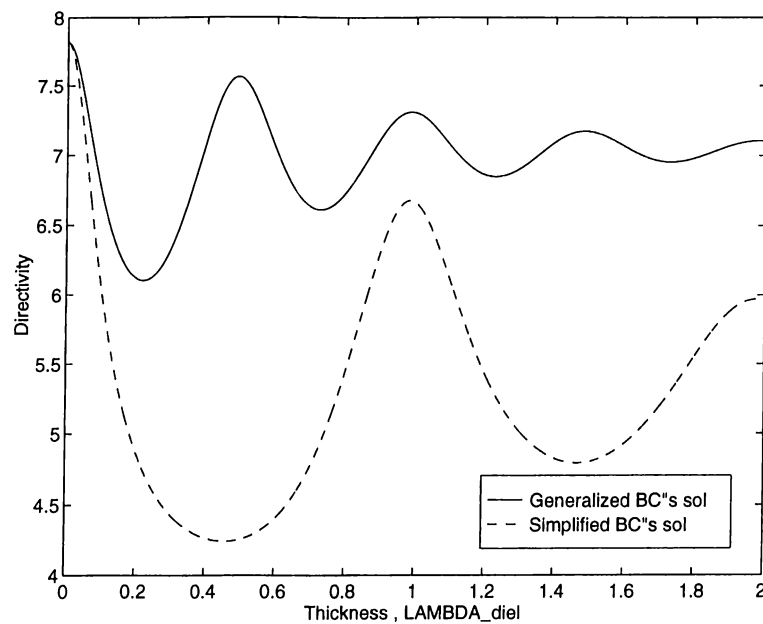

Figure 3.19: Directivity versus Thickness for a circular dielectric radome $ka = 62.8, kr_0 = 0, kb = 5, \tilde{\epsilon}_r = 4 + i$.

Figure 3.20: Directivity versus Thickness for a circular dielectric radome $ka = 62.8, kr_0 = 0, kb = 5, \tilde{\epsilon}_r = 4 + i0.5$.

Figure 3.21: Directivity versus Thickness for a circular dielectric radome $ka = 62.8, kr_0 = 0, kb = 10, \tilde{\epsilon}_r = 4 + i0.5$.
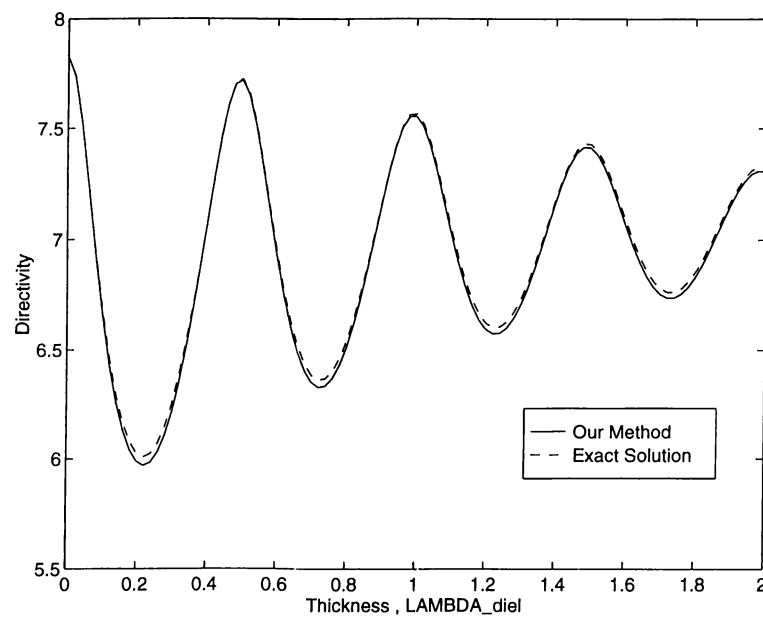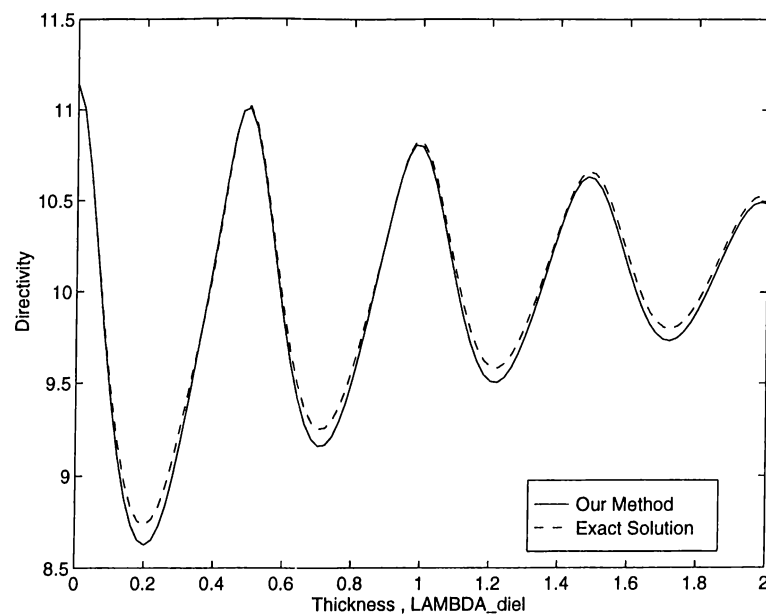
Figure 3.22: Directivity versus Thickness for a circular dielectric radome $ka = 62.8, kr_0 = 0, kb = 15, \tilde{\epsilon}_r = 4 + i0.5$.

Figure 3.23: Directivity versus Thickness for a circular dielectric radome $ka = 62.8, kr_0 = 0, kb = 20, \tilde{\epsilon}_r = 4 + i0.5$.
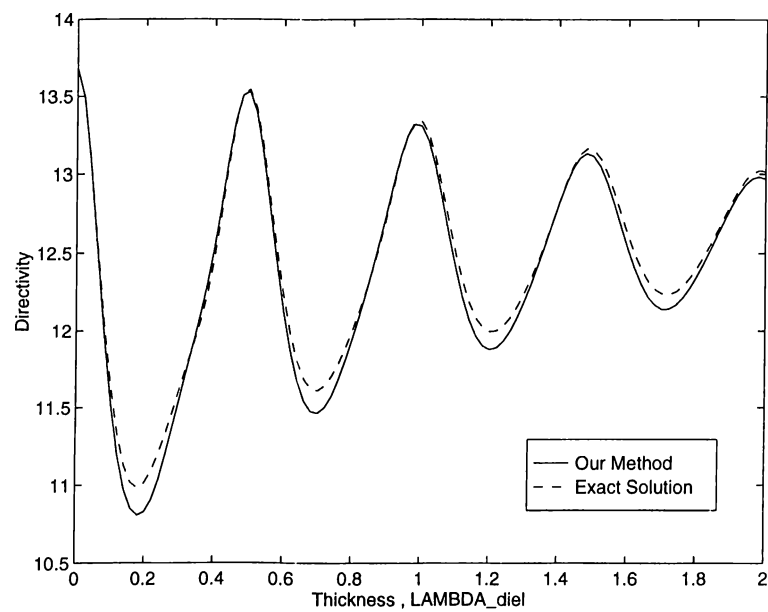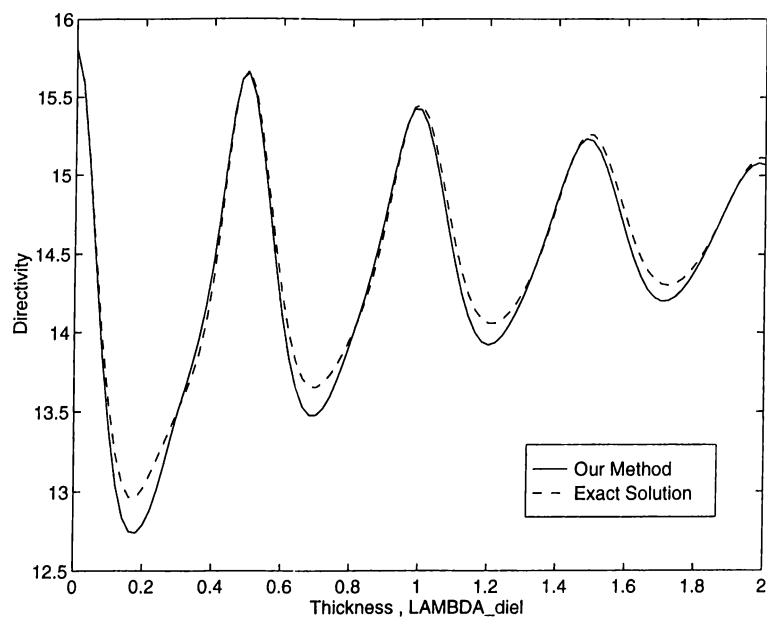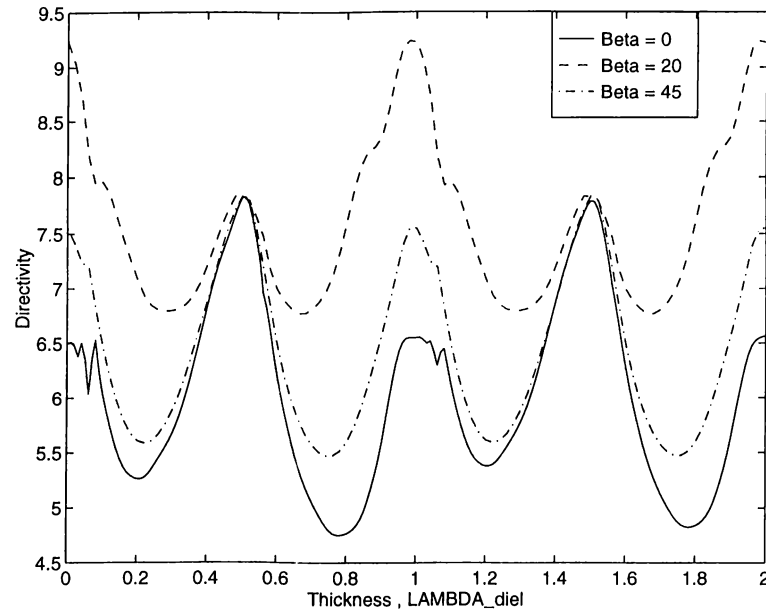
Figure 3.24: Directivity versus Dielectric Thickness for a circular metal-dielectric radome.
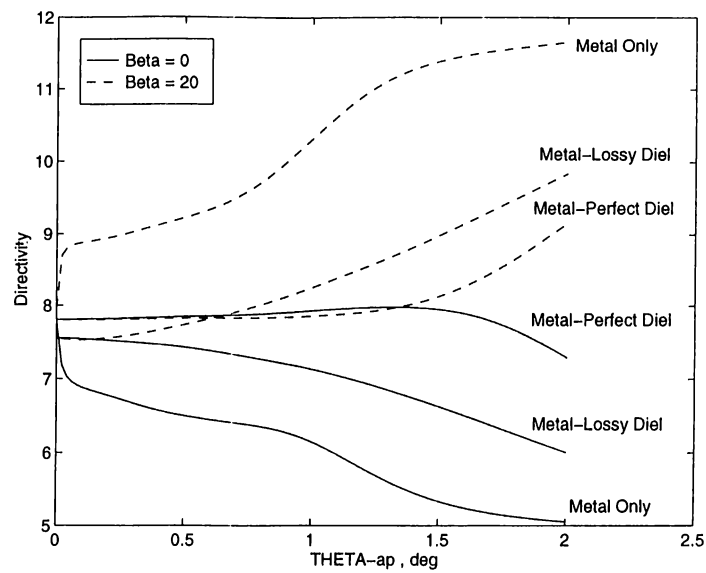
Figure 3.25: Directivity versus Angular Width of metal strips for a circular metal-dielectric radome.
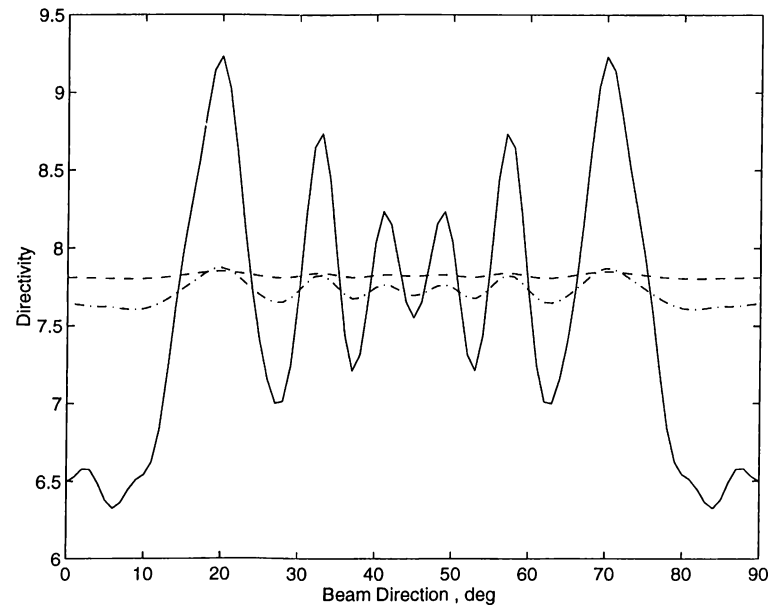
Figure 3.26: Directivity versus Beam Direction for a circular radome: $\theta_{ap} = 0.5°$;solid:metal in free space;dashed:metal-diel $\tilde{\epsilon}_r = 4$;dash dotted:metal-diel $\tilde{\epsilon}_r = 4 + i0.5$.

Figure 3.27: Directivity versus Beam Direction for a circular radome: $\theta_{ap} = 2°$;solid:metal in free space;dashed:metal-diel $\tilde{\epsilon}_r = 4$;dash dotted:metal-diel $\tilde{\epsilon}_r = 4 + i0.5$.

Figure 3.28: Directivity versus Beam Direction for a circular radome: $\theta_{ap} = 5°$;solid:metal in free space;dashed:metal-diel $\tilde{\epsilon_r} = 4$;dash dotted:metal-diel $\tilde{\epsilon_r} = 4 + i0.5$.
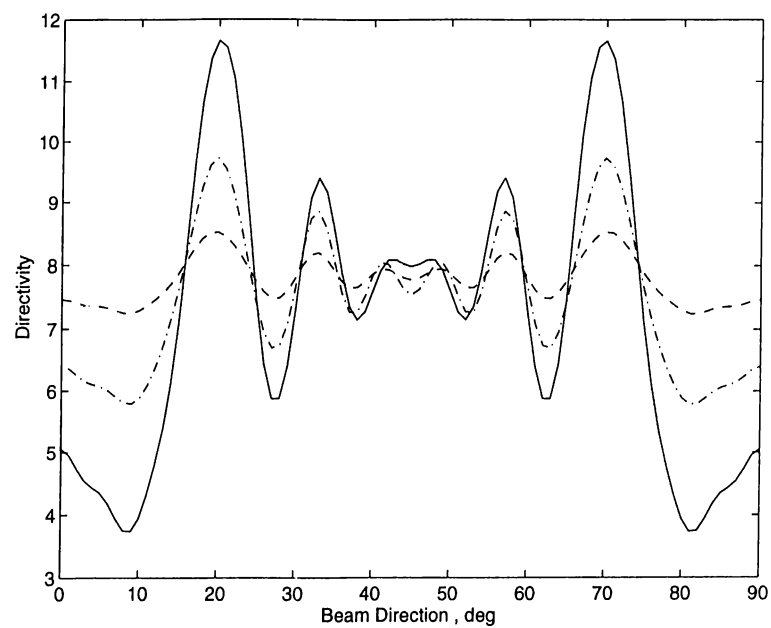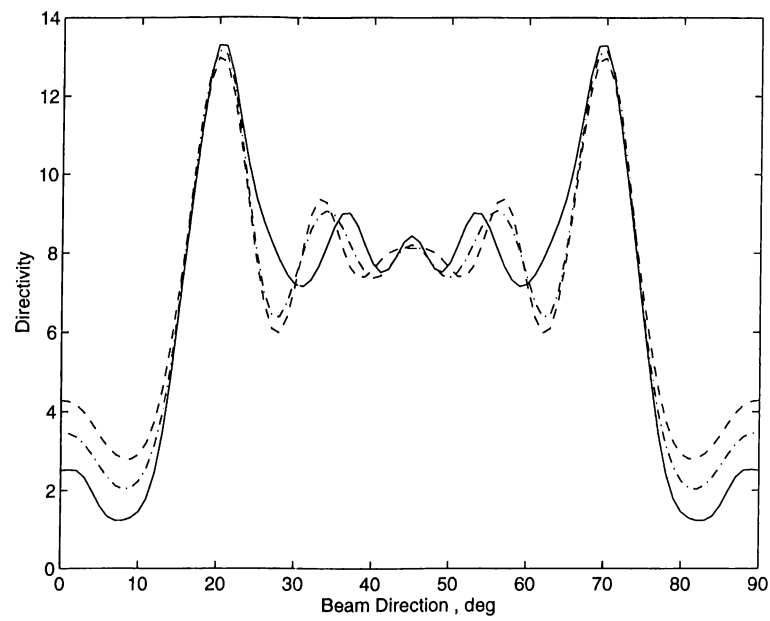
Chapter 4

CONCLUSIONS

In this thesis, the problem of electromagnetic wave penetration through a circular dielectric radome with gratings consisting of an array of periodic thin, lossy metal strips is considered. To the best of our knowledge, this is the first study made so far to solve such a problem with this approach.

The fields radiated by a complex line source are represented by modal cylindrical waves. Boundary conditions of a new generalized form, provided recently in the literature are used and manipulated according to our geometry to relate the outer fields to the inner ones and the analytic solution of the problem is obtained.

Results for the far zone fields and the directivity are calculated numerically for various structures as functions of the observation angle, the angular width of the metal strips and the beam orientation for metal gratings surrounded by vacuum. Also, presented are dependence of the directivity on the relative thickness of the dielectric layer for circular radome of metal-dielectric gratings. Finally, directivity variations with beam direction are presented. For the validation of the method results are generated and compared with the available ones for simple geometries.

According to our numerical data, the distortion of the main beam increases

and the directivity decreases with increasing number of strips and angular width in the case of metal gratings in free space. The directivity reveals a kind of resonant behavior as a function of the strip width d when the latter is about a multiple of the half wavelength in free space: $d \approx n\lambda/2$. It appears also that it is much better to use higher resistive strips to decrease the boresight error when the strip width $d < \lambda/2$.

The directivity shows considerable variations as a function of the beam direction. However, when a dielectric layer is inserted between the metal strips, the changes are much less observable especially for perfect dielectrics of half wavelength thickness. Unfortunately this is not valid for any width of the metal strips, and we are restricted to narrow ones ($d < \lambda/2$).

References

[1] W. C. Chew. *Waves and Fields in Inhomogeneous Media.* IEEE Press, New York, 1995.

[2] Jeng-Hwa Chang and Kuan-Kin Chan "Analysis of a Two-Dimensional Radome of Arbitrary Curved Surface," *IEEE Trans. Antennas Propagat.*, vol. 38, pp. 1565–1569, Oct. 1990.

[3] D. C. F. Wu and R. C. Rudduck "Plane Wave Spectrum-Surface Integration Technique for Radome Analysis," *IEEE Trans. Antennas Propagat.*, vol. 22, pp. 497–500, May 1974.

[4] P. D. Einziger and L. B. Felsen "Rigorous Asymtotic Analysis of Transmission Through a Curved Dielectric Slab," *IEEE Trans. Antennas Propagat.*, vol. 31, pp. 863– 869, Nov. 1983.

[5] J. J. Maciel and L. B. Felsen "Gaussian Beam Analysis of Propagation from an Extended Plane Aperture Distribution Through Dielectric Layers, Part I-Plane Layer," *IEEE Trans. Antennas Propagat.*, vol. 38, pp. 1607–1617, Oct. 1990.

[6] J. J. Maciel and L. B. Felsen "Gaussian Beam Analysis of Propagation from an Extended Plane Aperture Distribution Through Dielectric Layers, Part II-Circular Cylindrical Layer," *IEEE Trans. Antennas Propagat.*, vol. 38, pp. 1618–1624, Oct. 1990.

[7] L. B. Felsen, Subramaniam N., and K. Arichandran "Equivalence Relation Between Partial Angular Harmonic and Ray-Type Green's Functions for

Cylindrical Dielectric Layer," *IEEE Trans. Antennas Propagat.*, vol. 38, pp. 1273–1279, Aug. 1990.

[8] Anıl Bircan. "A Study of Line Source Fields Transmitted Through a 2D Circular Radome or a Slab,". Master's thesis, Bilkent University, Ankara Turkey, August 1996.

[9] R. G. Rojas and Z. Al-hekail "Generalized Impedance/Resistive Boundary Conditions for Electromagnetic Scattering Problems," *Radio Science*, vol. 24, pp. 1–12, Jan.-Feb. 1989.

[10] B. A. Thomas "Combined Resistive and Conductive Sheets," *IEEE Trans. Antennas Propagat.*, vol. 33, pp. 577–579, May 1985.

[11] E. Bleszynski, M. Bleszynski, and T. Jaroszewicz "Surface-Integral Equations for Electromagnetic Scattering from Impenetrable and Penetrable Sheets," *IEEE Antennas and Propagation Magazine*, vol. 35, pp. 14–25, Dec. 1993.

[12] R. C. Hall and R. Mittra "Scattering from a Periodic Array of Resistive Strips," *IEEE Trans. Antennas Propagat.*, vol. 33, pp. 1009–1011, Sep. 1985.

[13] R. C. Hall, R. Mittra, and K. M. Mitzner "Analysis of Multilayered Periodic Structures Using Generalized Scattering Theory," *IEEE Trans. Antennas Propagat.*, vol. 36, pp. 511–517, April 1988.

[14] R. Petit and G. Tayeb "Theoretical and Numerical Study of Gratings consisting of Periodic arrays of Thin and Lassy Strips," *J. Opt. Soc. Am.*, vol. 7, pp. 1686–1692, Sep. 1990.

[15] T. Oğuser, A. Altıntaş, and A. I. Nosich "Accurate Simulation of Reflector Antennas by the Complex Source-Dual Series Approach," *IEEE Trans. Antennas Propagat.*, vol. 43, pp. 793–801, Aug. 1995.

[16] G. Bouchitté and R. Petit "On the concept of a perfectly conducting material and a perfectly conducting and infinitely thin screen," *Radio Science*, vol. 24, pp. 13–26, Jan.-Feb. 1989.

[17] A. I. Nosich, V. B. Yurchenko, and A. Altıntaş. "Numerically Exact Analysis of a 2-D Variable-Resistivity Reflector Fed by a Complex Point Source,". to be published in IEEE Trans. Antennas Propagat., 1997.